Journal for ImmunoTherapy of Cancer

Cancer cell-autonomous overactivation of PARP1 compromises immunosurveillance in non-small cell lung cancer

Pan Juncheng [1,2,3] Adrien Joseph [1,2,3] Antoine Lafarge,[1,2,3]
Isabelle Martins,[1,2] Florine Obrist,[1,2,3] Jonathan Pol [1,2] Ester Saavedra,[1,2]
Sijing Li,[1,2,3] Allan Sauvat,[1,2] Giulia Cerrato,[1,2] Sarah Lévesque,[1,3] Marion Leduc,[1,2]
Oliver Kepp,[1,2] Sylvère Durand,[1,2] Fanny Aprahamian,[1,2]
Nitharsshini Nirmalathansan,[1,2] Judith Michels,[4] Guido Kroemer,[1,2,5]
Maria Castedo [1,2]

► Additional supplemental material is published online only. To view, please visit the journal online (http://dx.doi.org/10.1136/jitc-2021-004280).

PJ, AJ and AL are joint first authors.

Accepted 25 May 2022

Check for updates

For numbered affiliations see end of article.

Correspondence to
Dr Maria Castedo;
maria.castedo-delrieu@
sorbonne-universite.fr

Guido Kroemer;
kroemer@orange.fr

ABSTRACT

Background High activity of poly(ADP-ribose) polymerase-1 (PARP1) in non-small cell lung cancer (NSCLC) cells leads to an increase in immunohistochemically detectable PAR, correlating with poor prognosis in patients with NSCLC, as well as reduced tumor infiltration by cytotoxic T lymphocytes (CTLs). Intrigued by this observation, we decided to determine whether PARP1 activity in NSCLC cells may cause an alteration of anticancer immunosurveillance.

Methods Continuous culture of mouse NSCLC cells in the presence of cisplatin led to the generation of cisplatin-resistant PAR^high clones. As compared with their parental controls, such PAR^high cells formed tumors that were less infiltrated by CTLs when they were injected into immunocompetent mice, suggesting a causative link between high PARP1 activity and compromised immunosurveillance. To confirm this cause-and-effect relationship, we used CRISPR/Cas9 technology to knock out PARP1 in two PAR^high NSCLC mouse cell lines (Lewis lung cancer [LLC] and tissue culture number one [TC1]), showing that the removal of PARP1 indeed restored cisplatin-induced cell death responses.

Results PARP1 knockout (PARP1^KO) cells became largely resistant to the PARP inhibitor niraparib, meaning that they exhibited less cell death induction, reduced DNA damage response, attenuated metabolic shifts and no induction of PD-L1 and MHC class-I molecules that may affect their immunogenicity. PAR^high tumors implanted in mice responded to niraparib irrespective of the presence or absence of T lymphocytes, suggesting that cancer cell-autonomous effects of niraparib dominate over its possible immunomodulatory action. While PAR^high NSCLC mouse cell lines proliferated similarly in immunocompetent and T cell-deficient mice, PARP1^KO cells were strongly affected by the presence of T cells. PARP1^KO LLC tumors grew more quickly in immunodeficient than in immunocompetent mice, and PARP1^KO TC1 cells could only form tumors in T cell-deficient mice, not in immunocompetent controls. Importantly, as compared with PAR^high controls, the PARP1^KO LLC tumors exhibited signs of T cell activation in

WHAT IS ALREADY KNOWN ON THIS TOPIC

⇒ Poly(ADP-ribose) polymerase-1 (PARP1) is activated upon cisplatin-mediated DNA damage, and its hyperactivation mediates chemotherapy resistance in non-small cell lung cancer (NSCLC). Although high PARP1 activity is associated to poor prognosis of NSCLC, the impact of PARP1 on immunosurveillance has been elusive.

WHAT THIS STUDY ADDS

⇒ In our study, we show that cancer cell-specific knockout of PARP1, which is the most expressed member of this enzyme family in NSCLC, reverses cisplatin resistance. Moreover, in mouse models, knockout of PARP1 in NSCLC cells induces T lymphocyte-mediated tumor growth control coupled to signs of T cell activation in the local microenvironment.

HOW THIS STUDY MIGHT AFFECT RESEARCH, PRACTICE, OR POLICY

⇒ These results have implications for the mode of action of therapeutic PARP1 inhibitors and underscore a major impact of tumor cell metabolism on the cancer-immunity dialog.

the immune infiltrate such as higher inducible costimulator (ICOS) expression and lower PD-1 expression on CTLs.

Conclusions These results prove at the genetic level that PARP1 activity within malignant cells modulates the tumor microenvironment.

INTRODUCTION

Many chemotherapeutic agents induce DNA damage via direct interactions with chromatin and chromatin-binding proteins. This applies also to platinum-based cytoxicant including cis-diamminedichloroplatinum(II) (CDDP, best known as cisplatin), which directly

crosslinks DNA.[1–3] Logically, CDDP resistance may involve the upregulation of DNA damage repair.[4–7] Several years ago, we observed that a sizeable fraction of non-small cell lung cancer (NSCLC) cells that were selected for CDDP resistance by long-term culture in the continuous presence of CDDP were characterized by the enzymatic activation of poly(ADP-ribose) (PAR) polymerase-1 (PARP1),[8] which is involved in the repair of CDDP-induced DNA lesions.[9] Of note, this trait was conserved even after several months of culture in the absence of CDDP, reflecting an adaptive long-term alteration in tumor cell metabolism. Indeed, such cells contain higher levels of the PARP1 product PAR that can be detected by immunological methods.[8 10]

In NSCLC specimens, high level of immunohistochemically detectable PAR correlates with poor prognosis.[11] Since the levels of PARP1 expression and PAR do not correlate among each other, it is necessary to measure PAR instead of PARP1 mRNA or protein expression to establish such a prognostic relationship.[11] Like many other cancer types, NSCLC is affected in its prognosis by the density of the immune infiltrate.[12] Accordingly, we observed that high PAR levels were associated with scarce tumor infiltration by $CD8^+$ cytotoxic T lymphocytes (CTLs)[13] suggesting that PARP1 activity might influence the cancer-immune dialog. However, this conjecture has not been explored in mechanistic terms. Nonetheless, pharmacological PARP1 inhibitors can be advantageously combined with immune checkpoint inhibitors targeting cytotoxic T-lymphocyte associated protein 4 (CTLA-4)[14] or the programmed cell death protein 1 (PD-1)/programmed cell death ligand 1 (PD-L1) interaction,[15–17] as this has been reported in some clinical trials.

Here, we report the generation of PARP1 knockout cells from CDDP resistant PAR^{high} NSCLC cells. We show that this manoeuver reverses CDDP resistance, but renders the cells refractory to pharmacological PARP1 inhibition. Of note, this genetic manipulation profoundly affects the cancer-immune dialog, increasing the immune recognition of NSCLC in immunocompetent mice, hence improving their immunosurveillance. These findings have implications for the clinical anticorrelation between PAR levels and CTL infiltration.

MATERIALS AND METHODS

Cell culture conditions and chemicals. Lewis lung carcinoma (LLC) and tissue culture number one (TC1) murine lung cancer cell lines were purchased from the American Type Culture Collection (Rockefeller, Maryland, USA). PAR^{high} LLC and TC1 cell lines were obtained in vitro by prolonged culture of wild type LLC and TC1 cells with sublethal CDDP concentrations as previously described.[8 13] The knockout of PARP1 or STING was induced by means of the CRISPR/Cas-9 technology, according to the manufacturer's recommendations. Culture media and cell culture supplements were purchased from Gibco-Invitrogen Life Technologies (Carlsbad, Clifornia, USA). Wild-type LLC cells and their derivatives were cultured in Dulbecco's Modified Eagle's Medium (DMEM). Wild-type TC1 cells and their derivatives were cultured in glutamax RPMI-1640 medium supplemented with non-essential amino acids. Media for cell culture were supplemented with 10% fetal bovine serum, 100 U/mL penicillin G sodium salt, 100 mg/mL streptomycin sulfate. Cells were routinely maintained at 37°C under 5% CO_2 in T175, T75 and T25 flasks and seeded in appropriate supports (6, 12, or 96 wells plates) 24 hours before experimental determinations. All cells were amplified to generate liquid nitrogen stocks and, on thawing, never passaged for more than 1 month before use in experimental determinations. The cells were tested regularly for mycoplasma using MycoAlert Detection Kit (Lonza) and authenticated via PCR using nine short tandem repeat markers (IDEXX BioResearch). Niraparib and talazoparib were purchased from MedChemExpress and Selleck Chemicals, respectively. CDDP, DMXAA and methyl cellulose (viscosity 400 CP) came from Sigma-Aldrich.

CRISPR/Cas9-mediated knockout

CRISPR/Cas9-green fluorescent protein (GFP) plasmids targeting PARP1 (PARP1.a, target site: CGATGGGA AAGTCCCACACTGG; PARP1.b, target site: CGCCTGTC CAAGAAGATGGTGG), or specific for STING (target site: CTATAAGTCCCTAAGCATG), as well as control non-targeting plasmid were purchased from Sigma-Aldrich. Both PAR^{high} LLC cells and PAR^{high} TC1 cells plated in 6-well plates at a concentration of 0.25 million/well were transfected at 30%–40% confluence with CRISPR plasmids by means of the Fugene transfection reagent (Qiagen). Similarly, $PARP1^{KO}$ TC1 cells were transfected with CRISPR plasmid specific for STING. Twenty-four hours later, cells were trypsinized and transiently expressing GFP cells were sorted by cytofluorometry in 96-well plates (1 cell/ well).

Immunoblotting

Cells were collected, washed twice with cold phosphate-buffered saline (PBS) and lysed in a buffer containing 50 mM Tris HCl pH 6.8, glycerol 10%, 2% SDS, 10 mM DTT and 0.005% bromophenol blue. Protein extracts (30 µg/lane) were separated on precast 4% to 12% SDS-PAGE gels (Invitrogen), followed by electro transfer to Immobilon membranes (Sigma-Aldrich) and immunoblotting with antibodies specific for PAR (10 hours; Calbiochem, Merck KGaA), PARP1 (Cell Signaling Technology Inc.), STING (Cell Signaling Signaling Technology), pTBK1 or TBK1 (Cell Signaling technology). An anti-β-actin antibody (mAb to beta actin, abcam) was used to monitor equal lane loading. Finally, membranes were incubated with appropriate horseradish peroxidase-conjugated secondary antibodies (Southern Biotech), followed by chemiluminescence detection with the SuperSignal West Pico reagent and either CL-XPosure X-rayfilms (both from Thermo Scientific-Pierce) or the

ImageQuantLAS 4000 Biomolecular Imager (GE Healthcare Life Sciences). Protein levels were quantified by densitometry using ImageJ software.

Cytofluorometric quantification of cell death

For the simultaneous quantification of plasma membrane integrity and mitochondrial transmembrane potential ($\Delta\psi m$), both adherent and non-adherent cells were collected, washed, and costained for 30 min at 37°C in 300 µL of culture medium containing 1 µg/mL propidium iodide (PI) which only incorporates into dead cells exhibiting plasma membrane rupture, and 40 nmol/L 3,3'-dihexyloxacarbocyanine iodide DiOC$_6$(3), a mitochondrial transmembrane potential sensitive dye (Molecular Probes-Invitrogen).[18–20] Cytofluorometric acquisitions were carried out on a Miltenyi cytofluorometer (MACSQuant Analyzer V.10), and analyses were performed by using the FlowJo software V.10.4.2 (TreeStar) on gating on events exhibiting normal forward scatter and side scatter parameters.

Mouse housing, cancer models and treatments

Eight-week-old female C57Bl/6 were purchased from Envigo France. Mice were maintained in specific pathogen-free conditions, at 25°C, with 12 hours light/12 hours dark cycles and fed ad libitum with free access to water. All animals were used under an approved protocol by the local Ethics Committee of Cordeliers Research Center (C2EA 05 no B-75-06-12, protocol no 21661) in accordance with the EU Directive 63/2010. To establish subcutaneously transplanted tumors, 5×10^5 LLC cells (C9 or C12 PAR^{high} clones; P15 or P17 PARP1^{KO} clones) or 3×10^5 TC1 cells (C5 or C7 PAR^{high} clones; P2 or P4 clones PARP1^{KO} clones; PS2, PS4 PARP1^{KO} STING^{KO} clones) were resuspended in 100 µL of PBS and inoculated into the right flank of C57Bl/6 mice under anesthesia with 2.5% isoflurane. For antibody mediated T cell depletion, mice received an intraperitoneal (i.p) injection of 100 µg anti-CD8a (clone YTS 169.4, BioXcell) and 100 µg anti-CD4 (clone GK1.5, BioXcell) antibodies or 200 µg of control isotype control (clone LFT-2, BioXcell) 2 days before tumor implantation. Then the antibodies were administered once a week. In order to inhibit the PD-1/PDL-1 interaction, anti-PD-1 (clone 29F.1A12, BioXcell) or isotype control (clone 2A3, BioXcell) was injected i.p. at 200 µg per mouse in 100 µL of PBS, 10 days after LLC cells injection. Then, the antibodies were administered twice a week.[21] To test the therapeutic effect of PARP1 pharmacological inhibition, niraparib was dissolved in 0.5% methyl cellulose (Sigma-Aldrich) in sterile water and stirred overnight when tumors attained an average volume of ~20 mm^3. Then, after the mice were randomized across the different groups, mice were administered 80 mg/kg niraparib orally in a volume of 100 µL per mice once daily for 5 days on and 2 days off per week. Control mice were administered 0.5% methyl cellulose. When used in combination, anti-PD-1 was injected 7 days after the first injection of niraparib, then twice a week.

Tumor growth was monitored via repeated measurements of the tumor size using a digital caliper. The volume of tumors was calculated using the following formula: tumor size (mm^3) = (length × width × height)/8×4/3 x π. Mean tumor growth curves were calculated by carrying over the last tumor size values of the mice that reached endpoint and interrupted when more than 50% of the group had reached endpoint. Mouse survival was carefully monitored. Tumor size exceeding 1500 mm^3, tumor ulceration, weight loss superior to 20% as compared with the beginning of the treatment and poor body condition were considered as endpoints.

Ex vivo blood processing and evaluation of T cell depletion

PAR^{high} and PARP1^{KO} tumors bearing mice were treated for 3 weeks with either control isotypes (CTL) or a combination of anti-CD8 and anti-CD4 antibodies (αCD8αCD4). Blood sampling was performed through retro-orbital sinus bleeding using a heparinized capillary tube. Blood was collected into a heparinized saline solution (30 U heparin/mL). Peripheral white blood cells were cleared of erythrocytes in 1X RBC lysis buffer (BioLegend) at room temperature for 10 min then washed twice in PBS. Surface staining of peripheral blood cells was performed with fluorescent antibodies: anti-CD-BV421 (145-2 C11), anti-CD8-PE (53-6.7) and anti-CD4-PerCP-Cy5.5 (RM4-5) purchased from BD Biosciences. Flow cytometry acquisition was performed on a MACSQuant Flow Cytometer (Miltenyi Biotec), and data analysis was conducted with the FlowJo software.

Ex vivo: tumor processing and phenotyping of immune infiltrate

LLC PAR^{high} and PARP^{KO} tumors were harvested, placed ice in gentle MACS C tubes (Miltenyi Biotec) containing DMEM and processed as previously described.[22] Briefly, tumors were dissociated with scissors, then enzymatically digested using Miltenyi Biotec mouse tumor dissociation kit and gentleMACS Octo Dissociator. Tumor homogenates were filtered through 70 µM MACS SmartStrainers (Miltenyi Biotec) and washed twice with ice-cold PBS. Then, after homogenization of bulk tumor cells in PBS at a concentration corresponding to 250 mg of the initial tumor weight /mL, 50 mg of the bulk tumor cell homogenates were stained with LIVE/DEAD Fixable Yellow dye (Thermo Fisher Scientific), and Fc receptors were blocked with anti-mouse CD16/CD32 (clone 2.4G2, BD Pharmingen). Surface staining of immune cells was performed with the following fluorochrome-conjugated antibodies: (1) 'Myeloid cell' panel: anti-CD45 APC-Fire750 (30 F-11, BioLegend), anti-Ly-6G PE (1A8, BD Pharmingen), anti-Ly-6C FITC (AL-21, BD Pharmingen), anti-CD11b V450 (M1/70, BD Pharmingen), anti-CD11c PE-Vio770 (REA754, Miltenyi Biotec), anti-CD80 PerCP-Cy5.5 (16–10A1, BD Pharmingen), and anti-I-A/E (MHC-II) APC (M5/114.15.2, BioLegend); (2) 'T-cell activation/exhaustion' panel: anti-CD3 APC V450 (17A2, Thermo Fisher Scientific), anti-CD8 PE (53–6.7, BD

Pharmingen), anti-CD4 PerCP-Cy5.5 (RM4-5, Thermo Fisher Scientific), anti-CD25 PE-Cy7 (PC61.5, Thermo Fisher Scientific), anti-inducible costimulator (ICOS) BV421 (7E.17G9, BD Pharmingen), and anti-PD-1 APC-Fire750 (29F.1A12, BioLegend). Cells were then fixed and permeabilized with anti-Foxp3 (eBioscience)/Transcription Factor Staining Buffer (Thermo Fisher Scientific). To complete the staining of the samples undergoing T cell immunophenotyping, cells were incubated with anti-Foxp3 FITC (clone FJK-16s, Thermo Fisher Scientific). Finally, stained samples were run through a BD LSR II flow cytometer and data acquired using BD FACSDiva 6.1.3 software (BD biosciences). Samples were then analyzed using FlowJo software.

Quantitative RT-PCR analysis of *IFNA1* and *IFNB1* mRNA expression

Total RNA was isolated using the Rneasy plus mini kit (Qiagen, Hilden, Germany) following manufacturer's instruction. Genomic DNA was digested using the RNase-Free DNase Set (Qiagen) according to manufacturer's guidance. Next, total RNA was reverse transcribed to cDNA using SuperScript IV VILO Master Mix (Thermo Fisher Scientific). A total of 1–2.5 µg of RNA were diluted in 16 µL of nuclease-free water and 4 µL of SuperScript IV VILO Master Mix were added. Reverse transcription was performed as previously described[23]: primer annealing at 25°C for 10 min, reverse transcription at 50°C for 10 min, and heat inactivation at 85°C for 5 min. Thereafter, IFNα1 (Mm03030145) or IFNβ1 (Mm00439552) were amplified using specific TaqMan Gene Expression assays (Thermo Fisher Scientific) using the TaqMan Fast Advanced Master Mix (Thermo Fisher Scientific) on the StepOnePlus RealTime PCR System (Applied Biosystems, Waltham, Massachusetts, USA). Running conditions were 50°C for 2 min, 95°C for 2 min followed by 40 cycles of target gene amplification (95°C for 1 s and 60°C for 20 s). Finally, threshold cycle (Ct) values of gene of interest were subtracted from Ct values of the housekeeping gene, PP1A, generating ΔCts; fold change of expression between PAR^{high} and $PARP1^{KO}$ samples was calculated using the formula: $2^{(-\Delta\Delta Ct)}$.

In vitro analysis of PD-L1, MHC Class I, MHC Class II and CALR expression by flow cytometry

LLC and TC1 cells were seeded in 96-well plates (1000 cells per well) in 100 µL growth medium and let adapt for 24 hours before treatment. Cells were then treated by different concentrations of niraparib for another 72 hours. Post-treated cells were collected in 96-well V-shape plates (Greiner-bio-one). Cells were first stained with DAPI (Thermo Fisher Scientific) for 15 min at 4°C in the dark as an exclusion dye to select viable (DAPI) cells, then washed and stained with an anti-mouse CD274 (PD-L1, MIH1, eBioscience), anti-mouse MHC Class I (H-2Kb, AF6-88.5.5.3, eBioscience), anti-mouse MHC Class II (I-A/I-E, M5/114.15.2, eBioscience) monoclonal antibody, anti-CALR (ab2907, Abcam) for another 25 min

at 4°C in the dark. After staining, cells were fixed with 4% PFA and kept at 4°C. Flow cytometry acquisition was performed on a MACSQuant (Miltenyi Biotec), and data analysis was conducted with the FlowJo software.

Cytofluorometric analysis of polyploidy

LLC cells were seeded in 12-well plates (20 000 cells per well). After 24 hours adaptation, cells were treated with niraparib for 72 hours. Cells were then collected and fixed with cold 80% ethanol. Samples were kept at −20°C overnight and stained with FxCycle ^{TM} PI/RNase Staining Solution (Invitrogen) following all manufacturers instructions. Flow cytometry acquisition was performed on a MACSQuant (Miltenyi Biotec), and data analysis was conducted with the FlowJo software, as described.[24 25]

DNA damage foci measured by immunofluorescence detection of phosphorylated histone H2AX (γH2AX)

Cells were seeded into 384 wells black microplates (500 cells/well) and cultured in normal conditions or in the presence of niraparib (1.5, 3, 6, 12, 24 µM) for 72 hours. Alternatively, cells were seeded into 384 wells black microplates (1000 cells/well) and cultured in normal conditions or in the presence of CDDP (2.5, 5, 10, 20 µM) for 24 hours. After washing twice with PBS, plates were fixed with 4% PFA/PBS containing Hoechst 33 342 (2 µg/mL) for 10 min which was used for nuclear conterstaining, washed twice with PBS and incubated with quenching solution (2.67 g NH_4Cl in 1 L PBS, pH 7.4) for 5 min. Thereafter, cells were washed with PBS, permeabilized with 0.1% Triton-X 100 for 10 min, and rinsed twice with PBS. Plates were blocked with 2% BSA in PBST (PBS, 0.01% Tween-20; v:v) for 30 min before incubation with anti-γH2AX (Ser139; clone JBW301) antibody (Sigma Aldrich) overnight at 4°C. Then the cells were rinsed twice with PBS and incubated with secondary antibody for 30 min at room temperature in the dark. After additional washing steps, 50 µL PBS were added to each well. Cells micrographs were acquired by means of an IXM XLS automated fluorescent microscope (Molecular Devices) equipped with a Plan Apo 20X objective using the DAPI and GFP filter sets, and subsequent image analysis was performed using the *EBImage* package form the R bioconductor repository. Briefly, nuclei masks were created using the Hoechst 33 342 signal, and used to measure the nuclear γH2AX intensity. γH2AX foci count was determined from the dots masks obtained by thresholding the top-hat-filtered GFP image.[26]

Sample preparation for metabolome analysis

LLC or TC1 cells were seeded in 6-well plates and cultured for 24 hours in complete medium. Forty-eight hours before extraction, medium was changed and cells were cultured either in complete medium alone or complete medium with niraparib (five replicates per condition). Subsequently, cells were washed five times with cold PBS before rinsing with water, and then scraped in 500 µL of methanol (90%)-water (10%). Then, 100 µL

of chloroform were added. After centrifugation (10 000 g, 10 min, 4°C), the whole supernatant was evaporated at 40°C to obtain dried extracts. Three hundred µL of methanol were added on dried extract and split in two 150 µL fractions for gas chromatography-mass spectrometry (GC-MS) and liquid chromatography-mass spectrometry (LC-MS) analyses respectively. For GC-MS assay, methanol solubilized aliquots were transferred to glass tubes and solvent was evaporated. A total of 50 µL of methoxyamine (20 mg/mL in pyridine) were added on dried extracts, then stored at room temperature in dark, during 16 hours. The day after, 80 µL of MSTFA were added and final derivatization occured during 30 min at 40°C. Samples were then transferred to vials and directly injected into GC-MS. After a second evaporation round, LC-MS dried extracts were solubilized in 300 µL of MilliQ water, centrifuged (10 min at 15 000 g, 4°C) and aliquoted in three microcentrifuge tubes (100 µL). Aliquots were transferred in ultra-high performance liquid chromatography (UHPLC) vials and injected into the UHPLC/MS or kept at −80°C until injection. Metabolomics was performed as previously described.[27 28]

Targeted analysis of cGAMP (2',3') by UHPLC coupled to a triple quadrupole (QQQ) mass spectrometer

Dry pellets obtained from LLC or TC1 cells cultured for 24 hours in complete medium were recovered with 500 µL of Methanol, vortexed 5 min (2500 rpm) and centrifugated (10 min, 15 000 g, 4°C). A total of 200 µL of supernatant were transferred in microtubes and evaporated. Dry samples were spiked with 150 µL of MilliQ water, vortexed and centrifugated. A total of 50 µL of water were transferred in injection vials and spiked with 5 µL of formic acid, before direct injection into LC-MS. Targeted analysis was performed on an LC 1290 system (Agilent Technologies) coupled to a Agilent 6470 mass spectrometer equipped with an electrospray source operating in positive mode. A total of 10 µL of sample were injected on an Agilent's Column Zorbax XDB-C18 (4.6×50 mm, particle size 1.8 µm) heated at 40°C. The autosampler was kept at 4°C. The mobile phases were water (0.2% of acetic acid) (A) and acetonitrile (B). MRM transitions followed the previously decribed protocole.[29]

Bioinformatic analysis

The relative mRNA expression of PARP isoforms in human NSCLC cell lines, normal lung tissues, and lung tumor tissues were retrieved from RNA-seq data contained in the Cancer Cell Line Encyclopedia dataset (https://sites.broadinstitute.org/ccle/), the Genotype-Tissue Expression (GTEx, https://gtexportal.org/home/) project, and The Cancer Genome Atlas (TCGA, https://www.cancer.gov/about-nci/organization/ccg/research/structural-genomics/tcga). To analyze differential expression, data from TCGA and GTEx datasets were uniformly converted to TPM (transcripts per million) format by the Toil process.[30]

Statistical analysis

Unless otherwise specified, all in vitro, experiments were independently repeated at least three times, yielding comparable results. Data were analyzed with GraphPad Prism software or Microsoft excel (Microsoft) and statistical significance was assessed by means of unpaired Student's t-test. In vivo, longitudinal analyses of tumor growth data were carried out by linear mixed-effect modeling on tumor sizes. Linear mixed-effects models were applied for longitudinal comparison of tumor growth curves with the TumGrowth web tool[31] (https://github.com/kroemerlab/TumGrowth). For graphing, tumor growth data are represented in group-averaged tumor size alongside its SEM at each time point. Survival data are represented in Kaplan-Meier survival curves. Log-rank test was used to compute p values using GraphPad Prism software. The visualization and statistical analysis of gene expression data was based on R (V,3.6.3), ComplexHeatmap package (V.2.2.0), and ggplot2 package (V.3.3.3). P values were calculated by means of the Wilcoxon rank sum test. P values were considered significant when lower than 0.05. Bonferroni adjustment for multiple comparisons were used for metabolomic comparisons. Statistical significance was represented as following: $*/^{\#}p<0.05$, $**/^{\#\#}p<0.01$, $***/^{\#\#\#}p<0.001$.

RESULTS

Expression of different PARP isoforms in NSCLC

At the mRNA level, cell lines derived from primary and metastatic NSCLC express *PARP1* at much higher levels than any other members of the *PARP* gene family including those that possess enzymatic PARP activity (online supplemental figure S1A). Accordingly, in contrast to noncancerous lung tissue (online supplemental figure S1B), primary NSCLC adenocarcinomas and squamous carcinomas exhibit a clear dominance of *PARP1* expression over other members of the gene family (online supplemental figure S1C). Among the PARP isoforms endowed with the capacity of poly ADP-ribosylation (as opposed to mono ADP-ribosylation or other enzymatic activities), in particular PARP1, PARP2 and tankyrase/TNKS,[32] only PARP1 was significantly upregulated in NSCLC adenocarcinomas and squamous carcinomas as compared with normal adjacent tissues (online supplemental figure S1D,E). We therefore decided to focus our analysis on PARP1, which appears to be the most NSCLC-relevant protein of its family.

PARP1 knockout reverses CDDP resistance

Continuous culture of two murine NSCLC cell lines (LLC, and tumor cell-1 (TC1)) in the presence of CDDP led to the identification of cisplatin-resistant clones,[13] which often demonstrate the overactivation of PARP1, resulting in the intracellular accumulation of PAR, as determined by immunoblot analyses (online supplemental figure S2A,B). We chose two clones (LLC R7 and TC1 R18) for transfection with a CRISPR/Cas9-GFP vector that either

targets PARP1 or lacks a guidance RNA. The cells transiently expressing GFP were selected to derive clones that possess an elevated PARP1 activity, comparable to the parental clones (PAR^{high} cells), or that lack PARP1 expression and activity (PARP1^{KO} cells) (online supplemental figure S2C, figure 1A,B). The knockout of PARP1 sensitized the cells to death induction by CDDP. Thus, a higher proportion of PARP1^{KO} cells treated with CDDP tended to reduce their mitochondrial transmembrane potential (measured with DiOC$_6$(3)) and to incorporate the vital dye PI than PAR^{high} cells (figure 1C–F).

Altogether, these results establish that PARP1 overactivation is causally involved in CDDP resistance.

PARP1 knockout increases natural immunosurveillance

We previously demonstrated that, in patients with NSCLC, PAR^{high} tumors are less infiltrated by CD8$^+$ T lymphocytes than PAR^{low} tumors.[13] For this reason, we investigated whether PARP1 activity may affect anticancer immunosurveillance in mice. Representative PAR^{high} and PARP1^{KO} LLC clones were inoculated into the flanks of histocompatible C57Bl/6 mice, which were injected with either control isotypes or antibodies that deplete CD4$^+$ and CD8$^+$ T cells (figure 2A, online supplemental figure S3). PAR^{high} LLC tumors grew indistinguishably on immunocompetent and T cell-depleted mice (figure 2B,C, online supplemental figure S4A). However, the growth of PARP1^{KO} LLC tumors was accelerated by depletion of T lymphocytes, indicating that such cancers are under immunosurveillance (figure 2D,E, online supplemental figure S4B). Accordingly, cytofluorometric analyses demonstrated that the immune infiltrate of PAR^{high} and PARP1^{KO} LLC tumors were different. Although the absolute numbers of tumor-infiltrating CD45$^+$ leukocytes and CD3$^+$ cells did not change, the percentage of cells exhibiting the activation marker ICOS was increased among CD8$^+$ (but not CD4$^+$Foxp3$^-$ cells) and reduced among regulatory T cells (Tregs, defined as CD4$^+$Foxp3$^+$ cells, online supplemental figure S5 and figure 2F) from PARP1^{KO} LLC tumors as compared with PAR^{high} tumors. Moreover, the percentage of CD8$^+$ and CD4$^+$Foxp3$^-$ T cells expressing the exhaustion marker PD-1 was reduced in PARP1^{KO} LLC tumors in comparison to PAR^{high} tumors (figure 2F). These changes in ICOS and PD1 expression indicated as percentage of positive cells (figure 2F) were paralleled by similar shifts in the mean fluorescent intensity for such positive cells (online supplemental figure S6), underscoring the robustness of the results. Although upregulation of PD-1 might favor the action of PD-1 blockade, injection of an anti-PD-1 antibody failed to affect the growth of both PARP1^{KO} and PAR^{high} LLC tumors (online supplemental figure S7). Of note, PARP1^{KO} tumors were more infiltrated in activated dendritic cells (CD45$^+$CD11c$^+$MHCI-I^{high} cells, online supplemental figure S8) as compared with their PAR^{high} counterparts (figure 2G). In contrast, the frequency of CD45$^+$CD11b$^+$Ly6G$^-$Ly6C$^{low/intermediate}$ myeloid cells were not different among the two groups (figure 2G).

We also investigated the growth of PAR^{high} and PARP1^{KO} TC1 clones in immunocompetent versus T cell-deficient mice (figure 3A). Again, the growth of PAR^{high} tumors was not affected by the depletion of T cells. In sharp contrast, PARP1^{KO} TC1 clones were unable to form tumors in immunocompetent mice, but grew on T cell-depleted mice (figure 3B–E, online supplemental figure S9A,B). When immunocompetent mice had rejected the implantation of PARP1^{KO} TC1 cells (figure 3F), they subsequently also became resistant against PAR^{high} cells inoculated into the opposite flank (figure 3G,H, online supplemental figure S9C). These results demonstrate that PARP1^{KO} TC1 cells cause an anticancer immune response leaving a memory of the antigenic encounter.

In sum, these results demonstrate that the level of PARP1 activity modulates immunosurveillance. Cell-autonomous inhibition of PARP1 enhances the immune recognition of NSCLC cells.

On-target and off-targets effects of PARP inhibitors

We next wondered whether pharmacological PARP1 inhibition with niraparib, which is clinically approved for the treatment of platinum-resistant cancer,[33] could kill specifically PAR^{high} cancer cells. While PAR^{high} LLC cells died after a latency (7 days) in culture with niraparib (3 to 12 µM), PARP1^{KO} LLC cells only showed a marginal response at the highest niraparib dose (12 µM) (figure 4A,B), and similar effects were found when comparing the niraparib effects on PAR^{high} and PARP1^{KO} TC1 cells (figure 4C,D), or when replacing niraparib by talazoparib, another clinically approved PARP1 inhibitor (online supplemental figure S10). Thus, the knockout of PARP1 by genetic methods largely abolishes the cytotoxic effects of pharmacological PARP1 inhibitors. The culture of PAR^{high} LLC cells with PARP1 inhibitors for 3 days led to an increase in DNA damage foci measured by immunofluorescence detection of phosphorylated histone H2AX (γH2AX), and this effect was attenuated for PARP1^{KO} cells that lack the principal niraparib target (online supplemental figure S11A,B). Exposure of PAR^{high} LLC cells to niraparib caused an increase in nuclear size (online supplemental figure S11A) that reflects an increase in ploidy, as determined by cytofluorometric analyses of ethanol-fixed, RNAse-digested and PI-stained cells (online supplemental figure S11C,D). Again, the response of PARP1^{KO} cells to niraparib was much attenuated with respect to polyploidization (online supplemental figure S11). In sharp contrast, addition of CDDP to PARP1^{KO} LLC cells induced more γH2AX foci than in PAR^{high} cells (online supplemental figure S11E), in accord with the fact that PARP1^{KO} cells are more susceptible to CDDP-induced DNA damage.

Mass spectrometric metabolomics confirmed the preferential response of PAR^{high} LLC cells to niraparib (figure 5A). Of note, only two metabolites were significantly changed by the PARP1 knockout, namely NADH and γ-glutamylthreonine, which both were reduced as compared with PAR^{high} cells (online supplemental figure
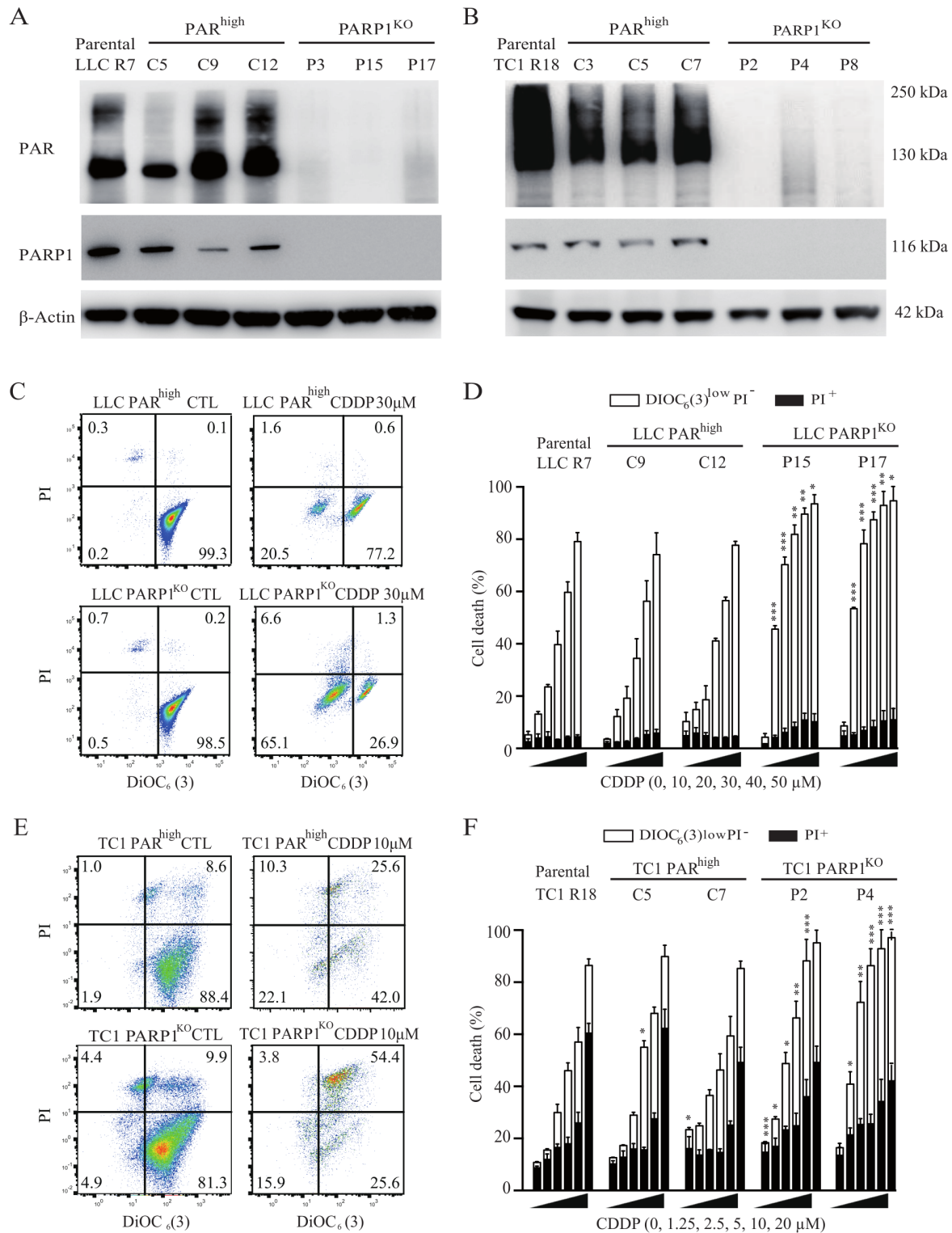
Figure 1 PARP1 hyperactivity is involved in cisplatin resistance. (A, B) Cisplatin-resistant R7 LLC (in A) and R18 TC-1 (in B) NSCLC clones were transfected with a CRISPR/Cas9-GFP vector that either targets PARP1 or lacks a guidance RNA. Parental clones and their CRISPR/Cas9 derivatives were processed for the immunoblotting-based assessment of PAR-containing proteins. Actin levels were monitored to ensure equal loading of lanes. (C–F) Parental cells and their CRISPR/Cas9 derivatives were maintained in control conditions or treated with the indicated concentrations of cisplatin for 72 hours. Then, cells were subjected to the cytofluorometric analysis of cell death-related parameters on costaining with the vital dye propidium iodide (PI) and the mitochondrial membrane potential-sensing dye DiOC$_6$ (3). C and E illustrate representative dot plots of LLC and TC1 cells respectively (numbers refer to the percentage of cells found in each quadrant), whereas D and F show quantitative data. White and black columns illustrate the percentage of dying and dead cells respectively (means±SEM, n=3). *P<0.05; **P<0.01; ***p<0.001 (Student's t-test), compared with equally treated parental R clones. GFP, green fluorescent protein; LLC, Lewis lung cancer; NSCLC, non-small cell lung cancer; PARP1, poly(ADP-ribose) polymerase-1.
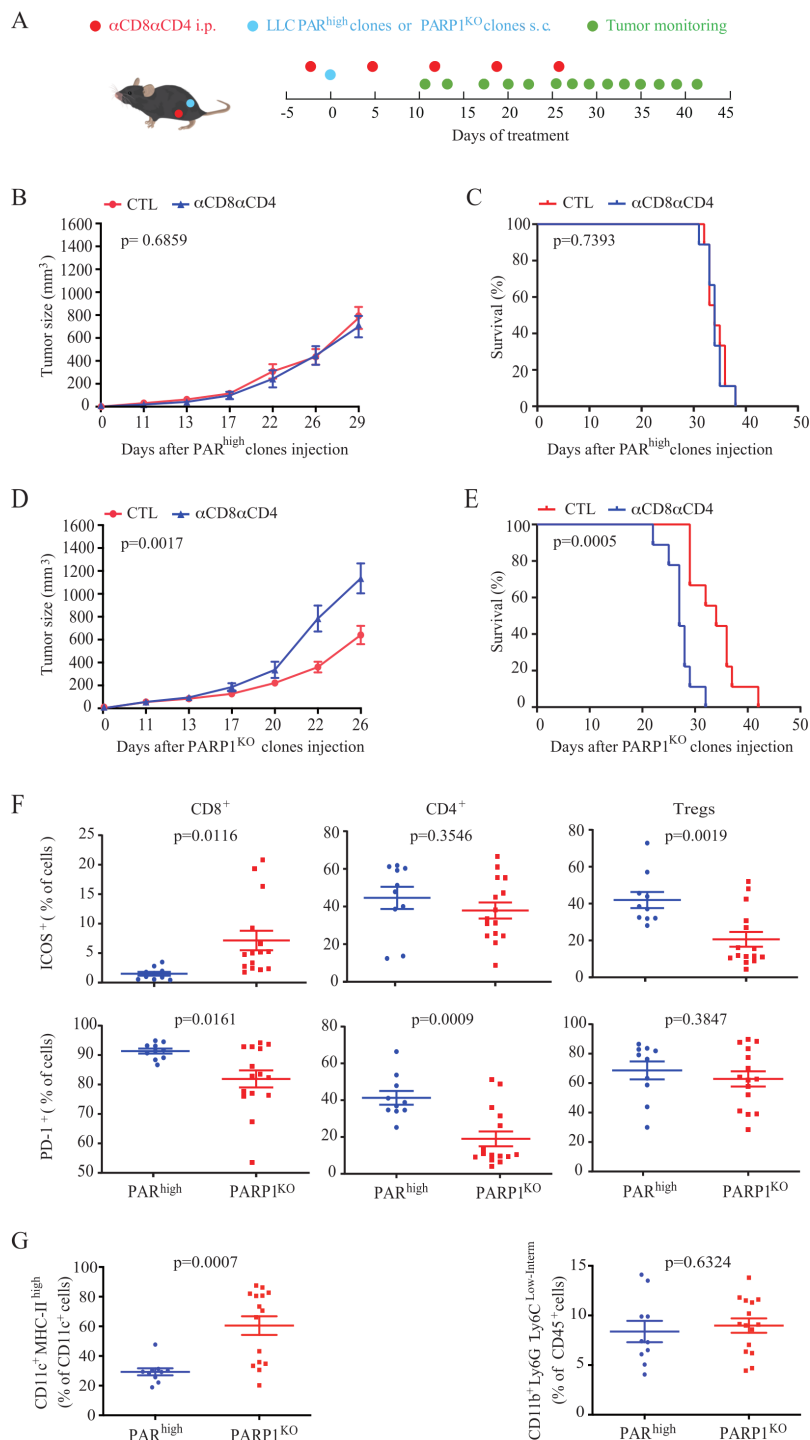
Figure 2 PARP1 knockout in LLC cancer cells impacts local immunosurveillance. (A) Experimental schedule of the implantation and treatment of syngeneic subcutaneous lung cancer in C57Bl/6 mice. 5×10⁵ PAR^high cells or PARP1^KO LLC cells were subcutaneously grafted into the flank of C57BL/6 mice. A combination of anti-CD8 and anti-CD4 (αCD8αCD4) neutralizing antibodies were intraperitoneally administrated 2 days before injection of tumor cells, then weekly. PAR^high CTL, PAR^highαCD8αCD4 and PARP1^KO CTL, n=10 mice; PARP1^KOαCD8αCD4, n=9 mice. (B–E) Mean tumor growth curves and Kaplan-Meier survival curves of mice subcutaneously grafted with PAR^high cells (B, C) or PARP1^KO cells (D, E). Tumor growth is reported as means±SEM. P values were calculated as compared with control (CTL) group (Wald test, type 2 ANOVA). For Kaplan-Meier, p values were determined by means of the log-rank test. (F, G) Characterization of the immune infiltrate in mouse lung cancers derived from PAR^high and PARP1^KO LLC cells. Immunocompetent C57BL/6 mice were injected subcutaneously with PAR^high and PARP1^KO clones (10 and 15 mice, respectively). In (F), dot plots illustrate the percentage of ICOS⁺ and PD-1⁺ cells among CD8⁺, CD4⁺ and T regulatory cells (Tregs) cells. In (G), percentage of CD11c⁺MHCII^high cells (among CD11c⁺) cells and CD11b⁺Ly6G⁻Ly6C^low/intermediate (among CD45⁺) cells. Means±SEM, p values were calculated by Student's t test as compared with PAR^high immune infiltrates. ANOVA, analysis of variance; CTL, cytotoxic T lymphocytes; ICOS, inducible costimulator; i.p, intraperitoneal; LLC, Lewis lung cancer; PAR, poly(ADP-ribose).
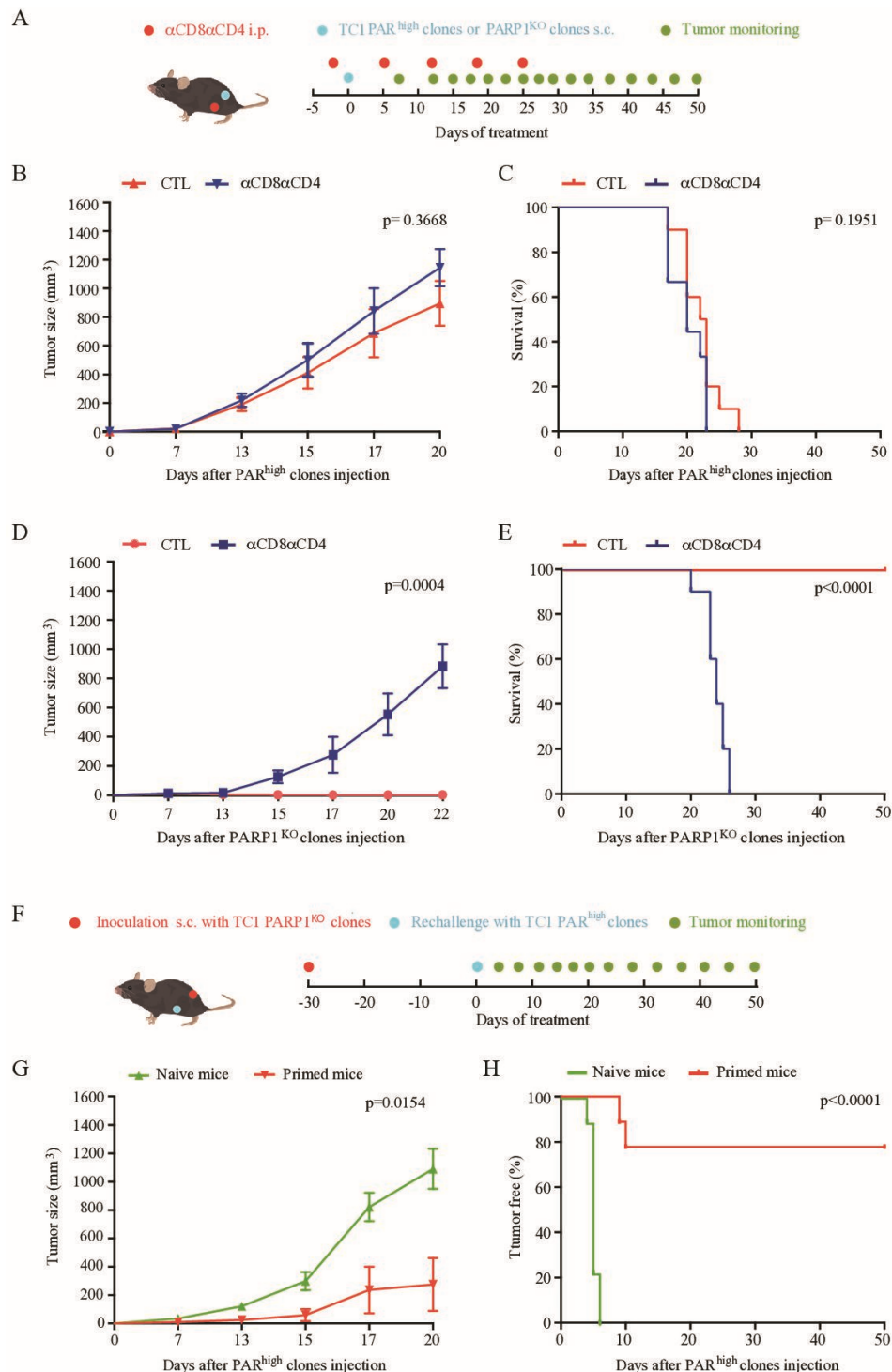
Figure 3 Knockout of PARP1 on TC1 cancer cells abolishes tumor formation in immunocompetent mice. (A) Schedule of the implantation and treatment of syngeneic subcutaneous TC1 cancer cells in naïve immunocompetent C57Bl/6 mice. 3×10^5 PAR^{high} cells or PARP1[KO] TC1 cells were subcutaneously grafted into C57BL/6 mice (PAR[high] CTL, PAR[high]αCD8αCD4 and PARP1[ko] CTL n=10 mice; PARP1[KO]αCD8αCD4, n=9 mice). Control isotypes or a combination of anti-CD8 and anti-CD4 neutralizing antibodies (αCD8αCD4) were intraperitoneally administrated 2 days before injection of tumor cells and then weekly. (B, C) Mean tumor growth and Kaplan-Meier survival curves of mice subcutaneously grafted with PAR^{high} cancer cells, respectively. (D, E) Mean tumor growth and Kaplan-Meier curves respectively of mice subcutaneously grafted with PARP1[KO] cells. (F–H) 3×10^5 PAR^{high} TC1 cells were injected into the left flank of immunocompetent C57BL/6 naïve tumor free mice or tumor free mice inoculated 1 month before with PARP1[KO] TC1 cells in the right flank (F). The evolution of tumor incidence over time was reported as tumor growth (G) and Kaplan-Meier (H) curves (naive and primed groups, n=8 and 9 mice, respectively). Error bars indicate SEM. P values were calculated as compared with CTL group (Wald test, type 2 ANOVA). For Kaplan-Meier, p values were determined by means of the log-rank test. ANOVA, analysis of variance; CTL, cytotoxic T lymphocytes; i.p, intraperitoneal; PARP1, poly(ADP-ribose) polymerase-1.
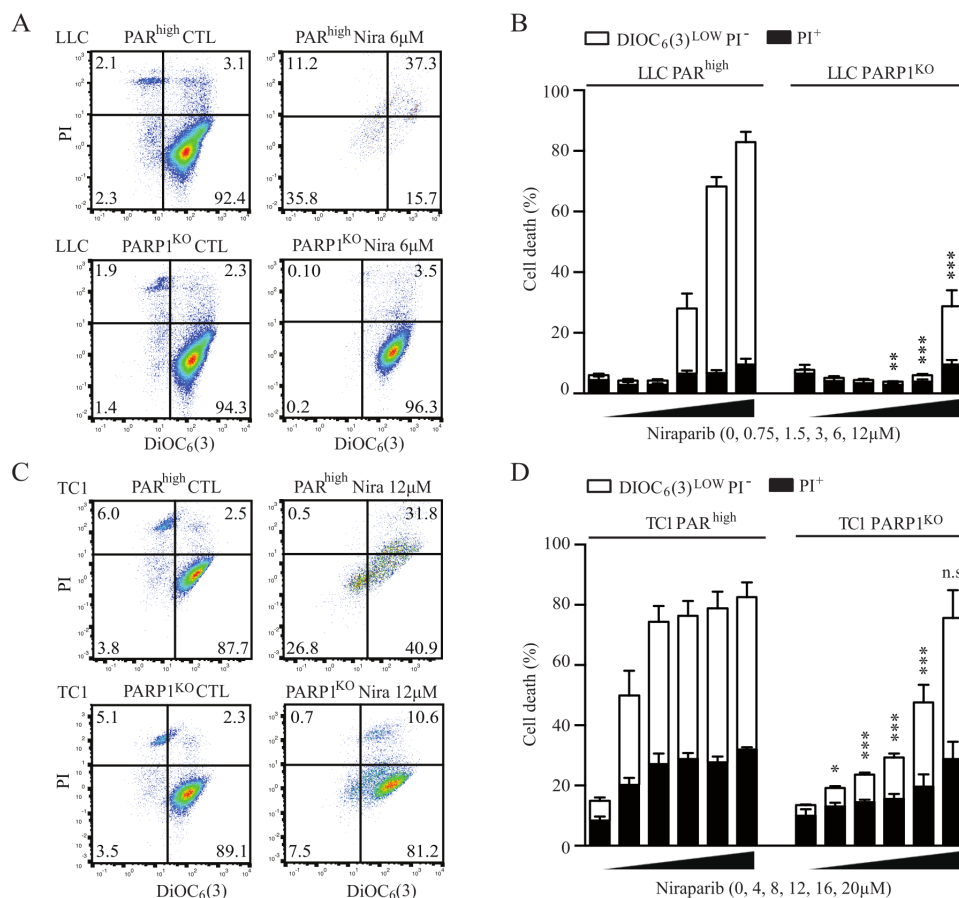
Figure 4 Niraparib preferentially kills cisplatin resistant PAR^high NSCLC cells. Mouse PAR^high and PARP1^KO LLC (A, B) or TC1 (C, D) cells were maintained in control conditions or treated with the indicated concentrations of niraparib for 7 days prior to the cytofluorometric assessment of apoptosis-related variables on costaining with propidium iodide (PI) and DiOC_6(3). Representative dot plots are shown in A and C whereas B and D show quantitative data (mean±SEM; n=3). *P<0.05; **p<0.01; ***p<0.001 (Student's t test) as compared with equally treated PAR^high cells. LLC, Lewis lung cancer; NSCLC, non-small cell lung cancer; PARP1, poly(ADP-ribose) polymerase-1.

S12). Volcano plots revealed that PAR^high cells responding to niraparib upregulated numerous nucleoside-relevant metabolites (such as guanosine, hypoxanthine, inosine, succinyladenosine, uridine, uridine monophosphate, xanthine) as well as Krebs cycle intermediates (fumarate, malate) (figure 5B). In contrast, only two metabolites (fructose-1–6-biphosphate, ureidosuccinate) were significantly downregulated by PAR^high LLC cells (figure 5B). Moreover, PARP1^KO cells showed a rather minor metabolic response to niraparib (figure 5C), in accord with the interpretation that PARP1 is the only relevant target of niraparib.

We also investigated whether PAR^high and PARP1^KO NSCLC cells might differ in their immunological characteristics,[34] determining the expression levels of PD-L1, MHC class I (H2K^b), MHC class II (I-A/E^b) molecules and calreticulin (CALR) by cytofluorometric staining. While there was no major difference in the mean fluorescence intensity between PAR^high and PARP1^KO LLC and TC1 cells, niraparib tended to increase the expression of these markers of immunogenicity more efficiently in PAR^high than in PARP1^KO cells (online supplemental figures S13, S14).

Altogether, these results demonstrate that clinically used PARP1 inhibitors have minor effects on cancer cells lacking PARP1, confirming that these treatments have scarce off-target effects.

Effects of PARP inhibitors on PARP1-deficient tumors in vivo

Since pharmacological PARP1 inhibition has little or no effects on PARP1^KO cells, it becomes possible to investigate potential effects of PARP inhibitors on immunosurveillance that occur independently from their inhibitory effects on PARP1 expressed by malignant cells (figure 6A). PAR^high tumors implanted in immunocompetent mice reduced their growth on treatment with niraparib, and this effect was similar in T cell-depleted mice (figure 6B, online supplemental figure S15A). Moreover, niraparib similarly extended the survival of immunocompetent and immunocompromised mice bearing PAR^high tumors (figure 6C), suggesting that the tumor growth-reducing effect of niraparib does not require the action of T lymphocytes. Of note, niraparib also reduced the growth of PARP1^KO cancers and extended animal survival. In this case, the magnitude of tumor growth reduction was affected by T cell depletion, and the acceleration of death
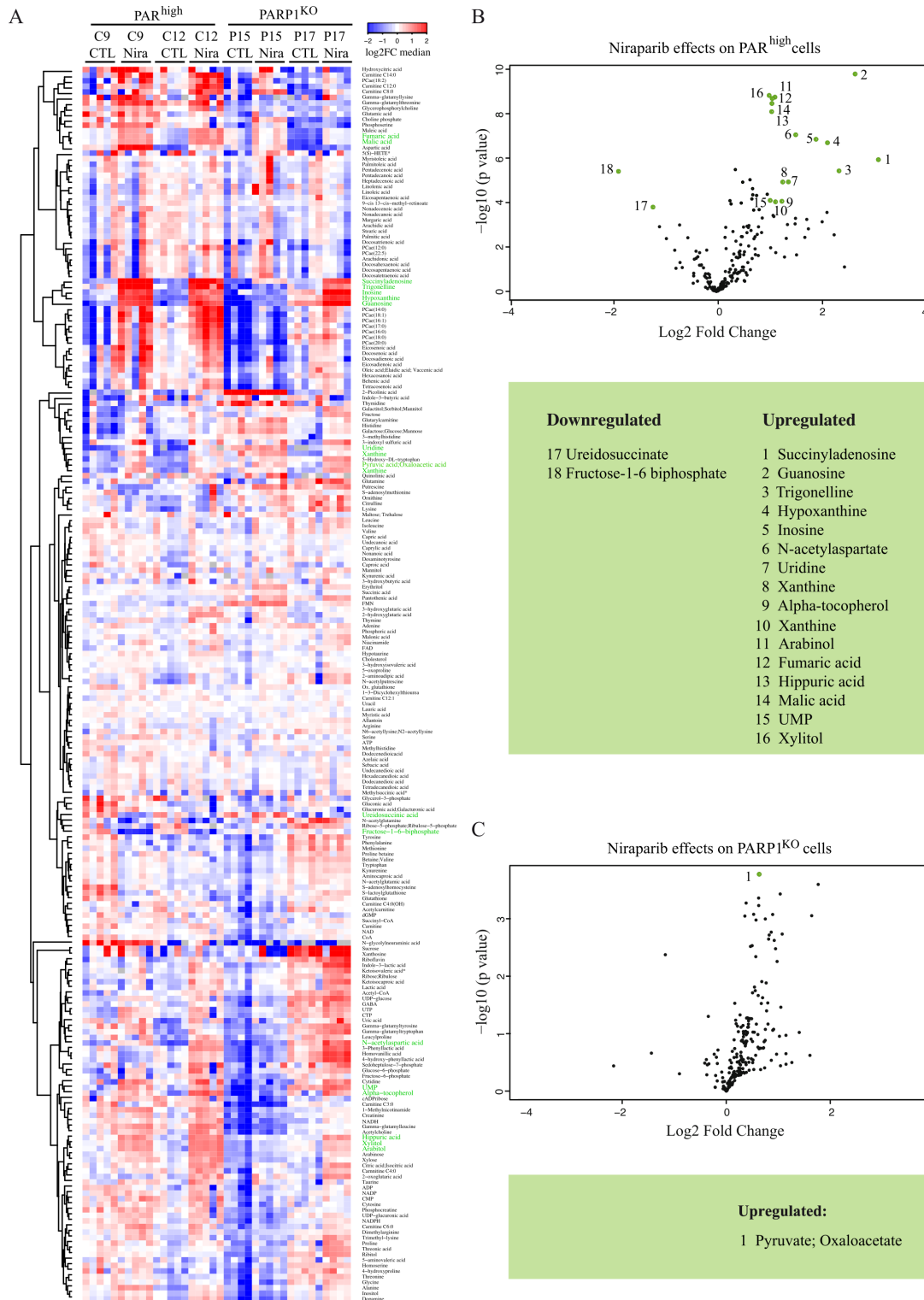
Figure 5 Metabolic response of PAR^high LLC lung cancer cells to niraparib. PAR^high and PARP1^KO LLC cells were cultured for 72 hours in normal condition or in the presence of niraparib (6 µM). (A) Heatmap represents metabolite differences between control condition and the presence of niraparib (Nira) shown as a color gradient (log2 scale). Five replicates per condition. Metabolites were clustered by means of the Ward method on the Euclidean distance matrix. In green, the name of metabolites whose level vary the most in the presence of niraparib. (B, C) Volcano plots identifying the metabolites whose levels vary significantly during treatment with niraparib in PAR^high (B) and PARP1^KO (C) cells, as compared with control (CTL) conditions. Niraparib and control metabolite levels were compared using t tests with Bonferroni adjustment for multiple comparisons. In B, green dots represent the metabolites which increase or decrease the most in PAR^high cells during the treatment with niraparib (adjusted p<0.05 and fold change >2). These metabolites are ordered in a table according to the descending fold-change. In C, only pyruvate/oxaloacetate increases significantly in PARP1^KO cells treated with niraparib as compared with CTL (adjusted p=0.0373 and fold change=1.587). CTL, cytotoxic T lymphocytes; LLC, Lewis lung cancer; PAR, poly(ADP-ribose).
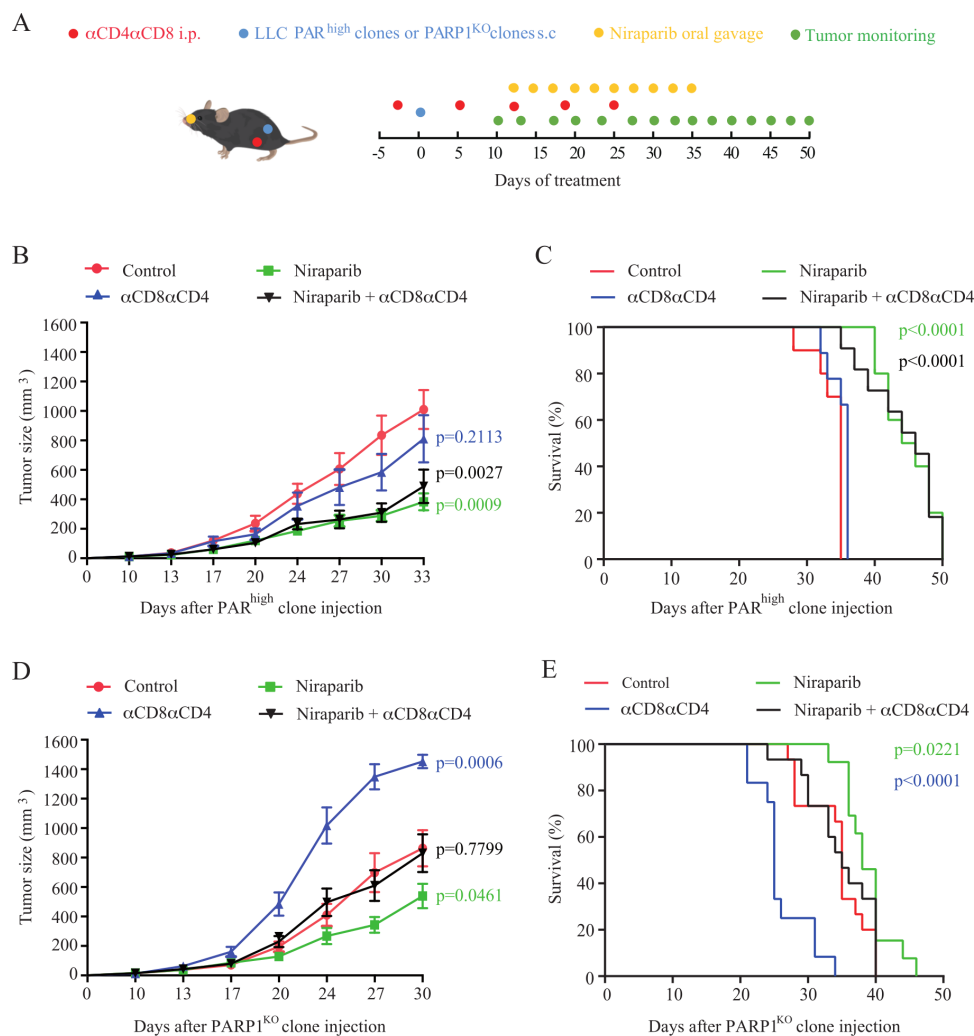
Figure 6 Effect of niraparib on tumors derived from PAR[high] and PARP1[KO] LLC cells. (A) Experimental schedule of the implantation and treatment of syngeneic subcutaneous lung cancer in C57Bl/6 mice. PAR^{high} cells and PARP1[KO] LLC cells were implanted into C57BL/6 mice with n mice per group and treated with vehicle or niraparib (80 mg/kg) along with an isotype control or a combination of anti-CD8 and anti-CD4 (αCD8αCD4) neutralizing antibodies. PAR[high] CTL, PAR[high] niraparib, PAR[high] niraparib+αCD8αCD4, n=10 mice; PAR[high]αCD8αCD4, n=9 mice; PARP1[KO] CTL and PARP1[KO] niraparib+αCD8αCD4, n=15 mice; PARP1[KO] niraparib, n=13 mice; PARP1[KO]αCD8αCD4, n=12 mice. (B–E) Mean tumor growth curves and Kaplan-Meier survival curves of mice subcutaneously grafted with PAR^{high} cells (B, C) or PARP[KO] cells (D, E). Tumor growth is reported as means±SEM over time. P values were calculated as compared with control (CTL) group (Wald test, type 2 ANOVA). For Kaplan-Meier, p values were determined by means of the log-rank test. ANOVA, analysis of variance; i.p, intraperitoneal; LLC, Lewis lung cancer; PAR, poly(ADP-ribose).

by injection of anti-CD4 and anti-CD8 antibodies was reversed by niraparib (figure 6D,E, online supplemental figure S15B). These latter results suggest that niraparib can mediate anticancer effects that do not require PARP1 expression in tumor cells and depend on T cells. The anticancer activity of niraparib on both PARP1[KO] and PAR[high] was not enhanced by PD-1 blockade (online supplemental figure S16).

Relationship between immununosurveillance of PARP1[KO] cells and cGAS/STING pathway activation

Subversion of the DNA damage response by inhibition of PARP reportedly activates the cyclic GMP-AMP (cGAMP) synthase/stimulator of interferon (IFN) genes (cGAS/STING) innate immune pathway in multiple cell types

secondary to the leakage of DNA into the cytosol.[35–39] This pathway leads to the induction of type-1 IFN expression, possibly explaining the recruitment of T cells in tumors.[40 41] Thus, the knockout of STING in cancer cells reduces or abolishes the therapeutic response to PARP inhibition.[35–41] Of note, both PAR[high] and PARP1[KO] NSCLC cells exhibited a low baseline level of TBK1 phosphorylation on serine 172, yet indistinguishably responded to the synthetic STING activator DMXAA by increasing TBK1 phosphorylation, demonstrating that they are, in principle, capable of activating the STING pathway (online supplemental figure S17). Moreover, in both mouse models of NSCLC (LLC and TC1), the knockout of PARP1 caused a decrease rather than an increase in
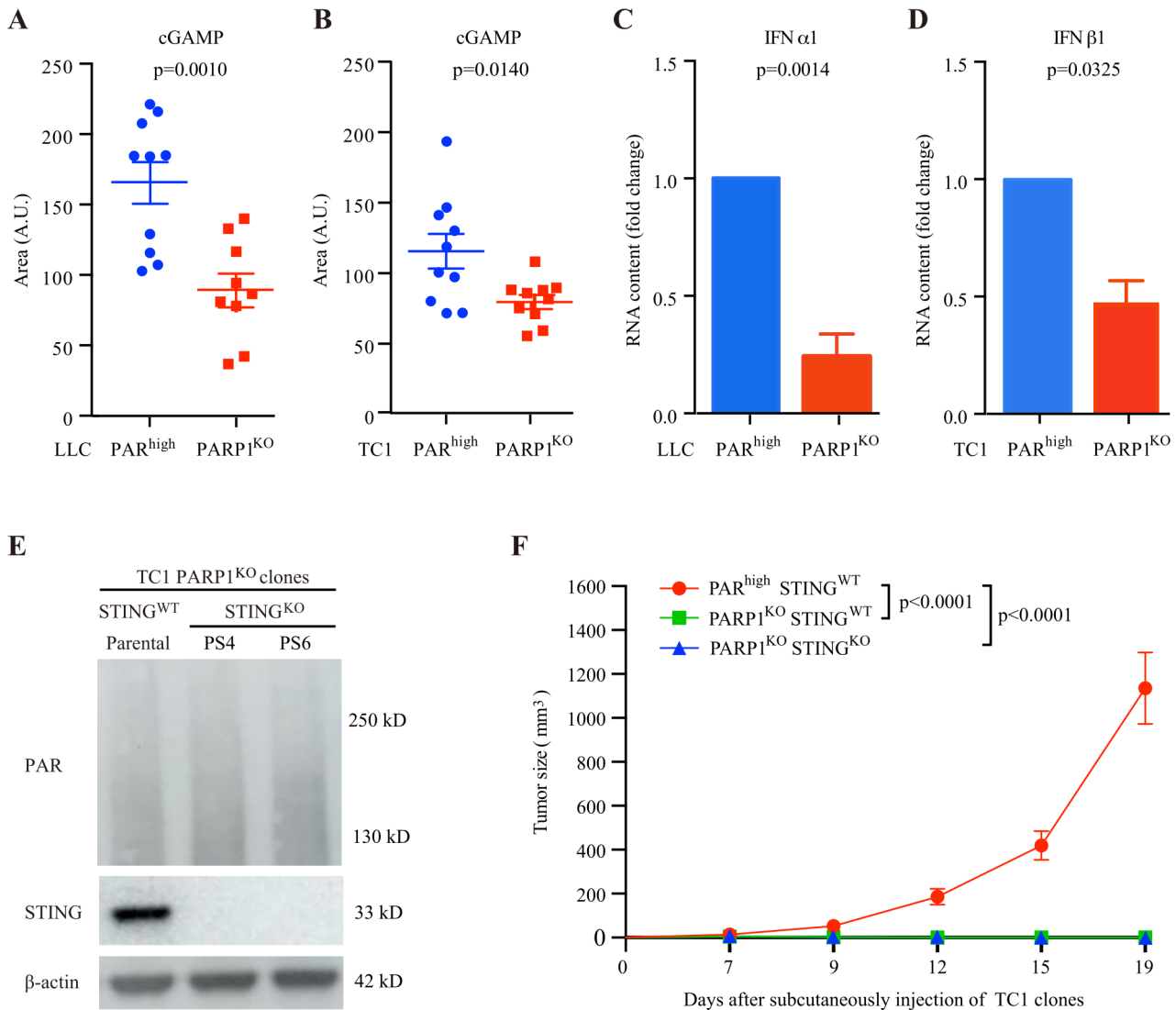
Figure 7 cGAS/STING pathway signaling and immune-dependent control of PARP1[KO] cells. (A,B) Levels of cGAMP in LLC (A) and TC1 (B) clones, cultured for 24 hours in normal culture medium. Mean±SEM Ten replicates per group except in LLC PARP1[KO] group (n=9–10 replicates). Data are shown as area of the metabolite peak. A.U: arbitrary unit. P values were calculated using the Student's t-test. (C, D) *IFNA1* and *IFNB1* expression was assessed in PAR[high] and PARP1[KO] LLC (C) and TC1 (D) cells by quantitative PCR using specific fluorescently labeled primer-probes sets. *GAPDH* was used as house-keeping gene. Fold changes of three independent experiments. Means±SEM. P values were calculated using the Student's t-test. (E) PARP[KO]STING[WT] TC1 parental cells and their PARP1[KO]STING[KO] derivatives (PS4 and PS6 clones) were cultured in normal culture medium and processed for the immunoblotting-based assessment of PAR-containing proteins and STING expression. Actin levels were monitored to ensure equal loading of lanes. (F) PAR[high]STING[WT], PARP1[KO]STING[WT] and PARP1[KO]STING[KO] TC1 cells were implanted subcutaneously into C57BL/6 mice (n=10 mice per group). Tumor growth was routinely monitored with a standard caliper and is reported as means±SEM. P values were calculated as compared with PAR[high]STING[WT] group (Wald test, type 2 ANOVA). Tumor growth is reported as means±SEM. ANOVA, analysis of variance; LLC, Lewis lung cancer; PAR, poly(ADP-ribose).

intracellular cGAMP concentrations, indicating that the cGAMP-producing enzyme cGAS was not activated by the genetic inhibition of PARP1 (figure 7A,B). In addition, PARP1[KO] cells failed to manifest an increase in the expression of the mRNA coding for the type-1 IFN alpha-1 or beta 1 (IFNA1, IFNB1) (figure 7C,D). Finally, the knockout of STING (figure 7E) failed to reverse the growth inhibition of PARP1[KO] TC1 cells in vivo, in C57Bl/6 mice (figure 7F). These results demonstrate that, in our specific system (which focuses on cisplatin-resistant NSCLC), overactivation of the cGAS/STING cannot explain the immune-dependent growth inhibition of PARP1[KO] cells.

DISCUSSION

PARP1 is an enzyme involved in the DNA damage response, and its activity is strongly induced by platinum-based chemotherapeutics.[42–45] We have shown in the past that PARP1 activity is durably increased in cancer cells

13

that have been selected by cultured in the presence of normally lethal CDDP doses, causing an increase in the PARP1 product PAR. Of note, in patients with NSCLC, a high abundance of PAR indicates poor prognosis, suggesting that PARP1 activity indeed is clinically relevant.[11] Here, we show that knockout of PARP1 eliminates PAR accumulation in cisplatin resistant NSCLC cells, indicating that it is indeed only PARP1 (and none of the other PARP isoforms) that accounts for PAR accumulation. Moreover, the deletion of *PARP1* reverses CDDP resistance, formally proving at the genetic level the importance of PARP1 activity.

Importantly, PAR^{high} cells were susceptible to cytotoxic effects of PARP1 inhibitors that were not observed with PARP1^{KO} cells, supporting that the pharmacological inhibitors that we characterized here (niraparib, talazoparib) are indeed highly specific for PARP1, lacking major off-target effects. In accord with this interpretation, niraparib caused DNA damage, polyploidization, metabolic effects (with a prominent upregulation of nucleosides, perhaps reflecting stalled DNA synthesis) and the upregulation of immune-relevant surface molecules (PD-L1, MHC class I and II, calreticulin) when added to PAR^{high} cells, but had no such effects on PARP1^{KO} cells, again supporting its specificity for PARP1. It is important to note that PARP1^{KO} cells lacked signs of spontaneous DNA damage, had a normal ploidy, were metabolically close-to-undistinguishable from their PAR^{high} counterparts, and did not show any upregulation of immune-relevant surface molecules. Hence, the long-term effects of the knockout of PARP1, which is followed by a phase of clonal selection, is not the same as the pharmacological inhibition of PARP1. This may reflect kinetic effects, namely chronic (genetic) inhibition allowing for adaptive mechanisms to come into action versus acute (pharmacological) inhibition. Moreover, enzymatic inhibition of PARP1 may cause the protein to stall DNA replication,[46–48] a phenomenon that would not occur in the absence of PARP1. Thus, the absence of PARP1 caused by the knockout of the gene may have different cellular effects than the drug-mediated inhibition of PARP1.

In this context, it appears intriguing that pharmacological PARP1 inhibition does reduce the growth of PAR^{high} tumors in a fashion that apparently is mediated by cell-autonomous effects since depletion of T cells (which are required for tumor growth reduction by anthracyclines or oxaliplatin[49]) does not interfere with this therapeutic effect. In sharp contrast, knockout of PARP1 did change the cancer-immune dialog in the sense that PARP1^{KO} tumors accelerated their growth on depletion of T cells (by combined injection of anti-CD4 and anti-CD8 antibodies), a phenomenon not seen for PAR^{high} tumors. An interesting difference was observed between LLC and TC1 NSCLC lines, knowing that TC1 are transduced with the E7 protein of human papilloma virus, rendering them highly antigenic.[50] PARP1^{KO} TC1 cells were unable to form tumors in immunocompetent mice and only did so after depletion of T cells. Mice that had been exposed to PARP1^{KO} TC1 cells visibly were immunized against TC1 epitopes since they became resistant against the inoculation of PAR^{high} TC1 cells that readily form tumors in naïve immunocompetent recipients. PARP1^{KO} LLC cells did form macroscopic cancers in immunocompetent mice, allowing to compare their immune infiltrate with that of PAR^{high} LLC tumors. Of note, PARP1^{KO} LLC tumors were more infiltrated in dendritic cells with high levels of MHC class-II expression than those found in PAR^{high} LLC tumors. Moreover, T cells infiltrating PARP1^{KO} LLC tumors exhibited signs of enhanced activation (enhanced percentage of ICOS$^+$ cells among CD8$^+$ T cells) and reduced exhaustion (reduced percentage of PD-1$^+$ cells among both CD4$^+$ CD8$^+$ T cells) when compared with T lymphocytes recovered from PAR^{high} LLC tumors. Moreover, a smaller percentage of Tregs infiltrating PARP1^{KO} LLC tumors expressed ICOS compared with Tregs infiltrating PAR^{high} LLC tumors. These results strongly suggest that the levels of PARP1 activation shape the tumor microenvironment, establishing a causal link. Thus, the clinical observation that PAR^{low} NSCLCs contain more CD8$^+$ T cells than PAR^{high} NSCLC does not only reflect a correlation, but likely reflects a cause-and-effect relationship.[13] However, no precise mechanistic explanation can be provided for the enhanced immunogenicity of PARP1^{KO} (or PAR^{low}) NSCLC. Indeed, when compared with their PAR^{high} counterparts, PARP1^{KO} cells did not exhibit any major changes in the immunogenic surface molecules studied nor in their metabolism. Future studies, for instance of the surface proteome or the immunopeptidome, must address this question.

Another observation requiring further investigation concerns the capacity of niraparib to reduce the growth of PARP1^{KO} tumors in mice. This effect cannot be explained by cell-autonomous effects because, at least in cell culture, PARP1^{KO} cells are resistant against the DNA damage-inducing and cytotoxic effects of niraparib. In contrast to our expectations, this effect seems to involve T lymphocytes. At this point, the mode of action of niraparib on PARP1^{KO} NSCLC remains enigmatic. Future studies must determine which host cell type (including fibroblasts or leukocytes other than T lymphocytes) or processes (such as angiogenesis) may be affected by niraparib to explain its paradoxical effects on PARP1^{KO} NSCLC.

Author affiliations
[1]Equipe 11 labellisée par la Ligue contre le Cancer, Université de Paris Cité, Sorbonne Université, Centre de Recherche des Cordeliers, INSERM UMR1138, Paris, France
[2]Metabolomics and Cell Biology Platforms, Gustave Roussy Cancer Campus, Villejuif, France
[3]Université Paris-Saclay, Faculté de Médecine, Le Kremlin-Bicetre, France
[4]Département de Médecine Oncologique, Gustave Roussy Cancer Campus, F-94805, Villejuif, France
[5]Institut du Cancer Paris CARPEM, Department of Biology, Hôpital Européen Georges Pompidou, Assitance Publique-Hôpitaux de Paris, Paris, France

Twitter Adrien Joseph @AdrienJoseph9

immunoblots. ES performed immunoblots. SL performed bioinformatic analyses. Immunofluorescence images were analyzed by AS, GC, ML and OK. SD, FA, and NN performed metabolome analyses. GK and MC conceived the project and wrote the manuscript. MC acts as guarantor. All of the authors critically reviewed and substantially improved the manuscript.

ORCID iDs
Pan Juncheng http://orcid.org/0000-0003-4626-3511
Adrien Joseph http://orcid.org/0000-0002-5278-8966
Jonathan Pol http://orcid.org/0000-0002-8355-7562
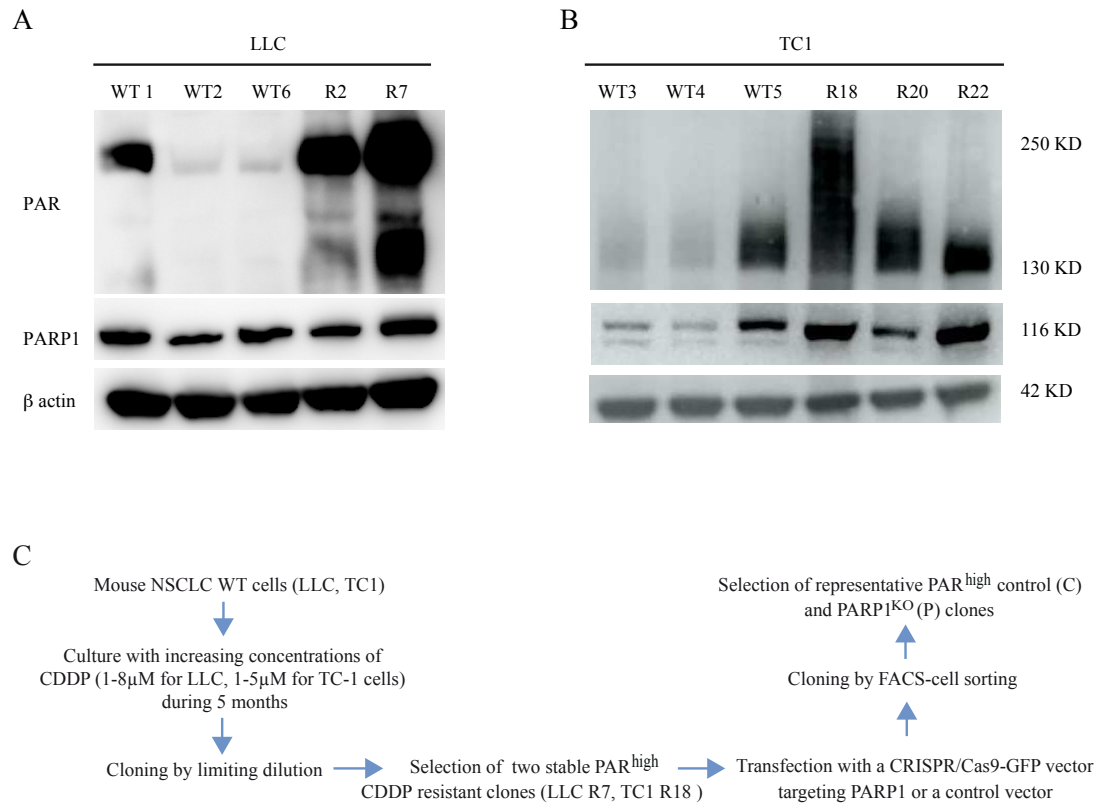Maria Castedo http://orcid.org/0000-0001-6855-3451

REFERENCES

1. Eastman A. The formation, isolation and characterization of DNA adducts produced by anticancer platinum complexes. *Pharmacol Ther* 1987;34:155–66.
2. Chaney SG, Campbell SL, Bassett E, *et al*. Recognition and processing of cisplatin- and oxaliplatin-DNA adducts. *Crit Rev Oncol Hematol* 2005;53:3–11.
3. Ohndorf U-M, Rould MA, He Q, *et al*. Basis for recognition of cisplatin-modified DNA by high-mobility-group proteins. *Nature* 1999;399:708–12.
4. Chaney SG, Sancar A. DNA repair: enzymatic mechanisms and relevance to drug response. *J Natl Cancer Inst* 1996;88:1346–60.
5. Metzger R, Leichman CG, Danenberg KD, *et al*. ERCC1 mRNA levels complement thymidylate synthase mRNA levels in predicting response and survival for gastric cancer patients receiving combination cisplatin and fluorouracil chemotherapy. *JCO* 1998;16:309–16.
6. Furuta T, Ueda T, Aune G, *et al*. Transcription-coupled nucleotide excision repair as a determinant of cisplatin sensitivity of human cells. *Cancer Res* 2002;62:4899–902.
7. Galluzzi L, Vitale I, Michels J, *et al*. Systems biology of cisplatin resistance: past, present and future. *Cell Death Dis* 2014;5:e1257.
8. Michels J, Vitale I, Galluzzi L, *et al*. Cisplatin resistance associated with PARP hyperactivation. *Cancer Res* 2013;73:2271–80.
9. Michels J, Vitale I, Senovilla L, *et al*. Synergistic interaction between cisplatin and PARP inhibitors in non-small cell lung cancer. *Cell Cycle* 2013;12:877–83.
10. Michels J, Vitale I, Saparbaev M, *et al*. Predictive biomarkers for cancer therapy with PARP inhibitors. *Oncogene* 2014;33:3894–907.
11. Michels J, Adam J, Goubar A, *et al*. Negative prognostic value of high levels of intracellular poly(ADP-ribose) in non-small cell lung cancer. *Ann Oncol* 2015;26:2470–7.
12. Fridman WH, Zitvogel L, Sautès–Fridman C, *et al*. The immune contexture in cancer prognosis and treatment. *Nat Rev Clin Oncol* 2017;14:717–34.
13. Joseph A, Juncheng P, Mondini M, *et al*. Metabolic features of cancer cells impact immunosurveillance. *J Immunother Cancer* 2021;9:e002362.
14. Higuchi T, Flies DB, Marjon NA, *et al*. CTLA-4 blockade synergizes therapeutically with PARP inhibition in BRCA1-deficient ovarian cancer. *Cancer Immunol Res* 2015;3:1257–68.
15. Domchek SM, Postel-Vinay S, Im S-A, *et al*. Olaparib and durvalumab in patients with germline BRCA-mutated metastatic breast cancer (MEDIOLA): an open-label, multicentre, phase 1/2, basket study. *Lancet Oncol* 2020;21:1155–64.
16. Lampert EJ, Zimmer A, Padget M, *et al*. Combination of PARP inhibitor olaparib, and PD-L1 inhibitor Durvalumab, in recurrent ovarian cancer: a proof-of-concept phase II study. *Clinical Cancer Research* 2020;26:4268–79.
17. Karzai F, VanderWeele D, Madan RA, *et al*. Activity of durvalumab plus olaparib in metastatic castration-resistant prostate cancer in men with and without DNA damage repair mutations. *J Immunother Cancer* 2018;6:141.
18. Galluzzi L, Vitale I, Kepp O, *et al*. Methods to dissect mitochondrial membrane permeabilization in the course of apoptosis. *Methods Enzymol* 2008;442:355–74.
19. Castedo M, Coquelle A, Vivet S, *et al*. Apoptosis regulation in tetraploid cancer cells. *EMBO J* 2006;25:2584–95.
20. Tajeddine N, Galluzzi L, Kepp O, *et al*. Hierarchical involvement of Bak, VDAC1 and Bax in cisplatin-induced cell death. *Oncogene* 2008;27:4221–32.
21. Lévesque S, Le Naour J, Pietrocola F, *et al*. A synergistic triad of chemotherapy, immune checkpoint inhibitors, and caloric restriction mimetics eradicates tumors in mice. *Oncoimmunology* 2019;8:e1657375.
22. Paillet J, Plantureux C, Lévesque S, *et al*. Autoimmunity affecting the biliary tract fuels the immunosurveillance of cholangiocarcinoma. *J Exp Med* 2021;218:e20200853.
23. Petrazzuolo A, Perez-Lanzon M, Martins I, *et al*. Pharmacological inhibitors of anaplastic lymphoma kinase (ALK) induce immunogenic cell death through on-target effects. *Cell Death Dis* 2021;12:713.
24. Deng J, Gutiérrez LG, Stoll G, *et al*. Paradoxical implication of BAX/BAK in the persistence of tetraploid cells. *Cell Death Dis* 2021;12:1039.
25. Senovilla L, Demont Y, Humeau J, *et al*. Image cytofluorometry for the quantification of ploidy and endoplasmic reticulum stress in cancer cells. *Methods Mol Biol* 2017;1524:53–64.
26. Perfettini J-L, Nardacci R, Bourouba M, *et al*. Critical involvement of the ATM-dependent DNA damage response in the apoptotic demise of HIV-1-elicited syncytia. *PLoS One* 2008;3:e2458.
27. Viltard M, Durand S, Pérez-Lanzón M, *et al*. The metabolomic signature of extreme longevity: naked mole rats *versus* mice. *Aging* 2019;11:4783–800.
28. Danlos F-X, Grajeda-Iglesias C, Durand S, *et al*. Metabolomic analyses of COVID-19 patients unravel stage-dependent and prognostic biomarkers. *Cell Death Dis* 2021;12:258.
29. Paijo J, Kaever V, Kalinke U. cGAMP quantification in virus-infected human monocyte-derived cells by HPLC-Coupled tandem mass spectrometry. *Methods Mol Biol* 2017;1656:153–66.
30. Vivian J, Rao AA, Nothaft FA, *et al*. Toil enables reproducible, open source, big biomedical data analyses. *Nat Biotechnol* 2017;35:314–6.
31. Enot DP, Vacchelli E, Jacquelot N, *et al*. TumGrowth: an open-access web tool for the statistical analysis of tumor growth curves. *Oncoimmunology* 2018;7:e1462431.
32. Barkauskaite E, Jankevicius G, Ahel I. Structures and mechanisms of enzymes employed in the synthesis and degradation of PARP-Dependent protein ADP-ribosylation. *Mol Cell* 2015;58:935–46.
33. Scott LJ. Niraparib: first global approval. *Drugs* 2017;77:1029–34.
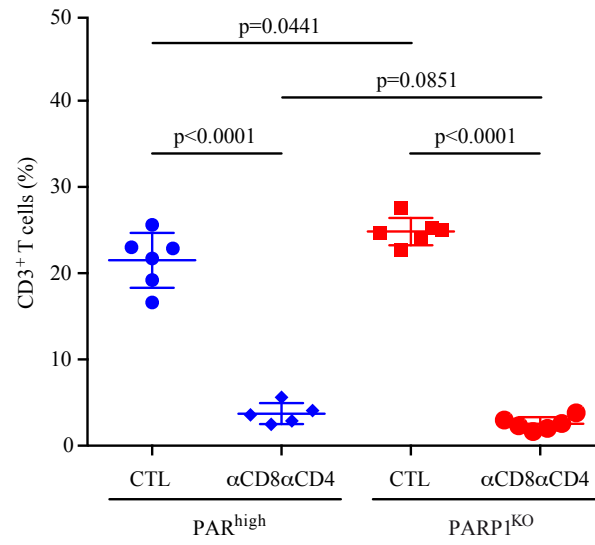34. Kroemer G, Galassi C, Zitvogel L, *et al*. Immunogenic cell stress and death. *Nat Immunol* 2022;23:487–500.

35 Shen J, Zhao W, Ju Z, *et al*. PARPi triggers the STING-dependent immune response and enhances the therapeutic efficacy of immune checkpoint blockade independent of BRCAness. *Cancer Res* 2019;79:311–9.

36 Sen T, Rodriguez BL, Chen L, *et al*. Targeting DNA damage response promotes antitumor immunity through STING-mediated T-cell activation in small cell lung cancer. *Cancer Discov* 2019;9:646–61.

37 Ding L, Kim H-J, Wang Q, *et al*. PARP inhibition elicits STING-dependent antitumor immunity in BRCA1-deficient ovarian cancer. *Cell Rep* 2018;25:2972–80.

38 Chabanon RM, Muirhead G, Krastev DB, *et al*. PARP inhibition enhances tumor cell–intrinsic immunity in ERCC1-deficient non–small cell lung cancer. *J Clin Invest* 2019;129:1211–28.

39 Reisländer T, Lombardi EP, Groelly FJ, *et al*. BRCA2 abrogation triggers innate immune responses potentiated by treatment with PARP inhibitors. *Nat Commun* 2019;10:3143.

40 Pantelidou C, Sonzogni O, De Oliveria Taveira M, *et al*. PARP inhibitor efficacy depends on CD8+ T-cell recruitment via intratumoral STING pathway activation in BRCA-Deficient models of triple-negative breast cancer. *Cancer Discov* 2019;9:722–37.

41 Bruand M, Barras D, Mina M, *et al*. Cell-autonomous inflammation of BRCA1-deficient ovarian cancers drives both tumor-intrinsic immunoreactivity and immune resistance via STING. *Cell Rep* 2021;36:109412.

42 Zhu G, Chang P, Lippard SJ. Recognition of platinum-DNA damage by poly(ADP-ribose) polymerase-1. *Biochemistry* 2010;49:6177–83.

43 Wang Q, Xiong J, Qiu D, *et al*. Inhibition of PARP1 activity enhances chemotherapeutic efficiency in cisplatin-resistant gastric cancer cells. *Int J Biochem Cell Biol* 2017;92:164–72.

44 Prasad CB, Prasad SB, Yadav SS, *et al*. Olaparib modulates DNA repair efficiency, sensitizes cervical cancer cells to cisplatin and exhibits anti-metastatic property. *Sci Rep* 2017;7:12876.

45 Cheng H, Zhang Z, Borczuk A, *et al*. PARP inhibition selectively increases sensitivity to cisplatin in ERCC1-low non-small cell lung cancer cells. *Carcinogenesis* 2013;34:739–49.

46 Kedar PS, Stefanick DF, Horton JK, *et al*. Increased PARP-1 association with DNA in alkylation damaged, PARP-inhibited mouse fibroblasts. *Mol Cancer Res MCR* 2012;10:360–8.

47 Murai J, Huang S-yinN, Das BB, *et al*. Trapping of PARP1 and PARP2 by clinical PARP inhibitors. *Cancer Res* 2012;72:5588–99.

48 Helleday T. The underlying mechanism for the PARP and BRCA synthetic lethality: clearing up the misunderstandings. *Mol Oncol* 2011;5:387–93.

49 Zitvogel L, Galluzzi L, Smyth MJ, *et al*. Mechanism of action of conventional and targeted anticancer therapies: Reinstating immunosurveillance. *Immunity* 2013;39:74–88.

50 Lin KY, Guarnieri FG, Staveley-O'Carroll KF, *et al*. Treatment of established tumors with a novel vaccine that enhances major histocompatibility class II presentation of tumor antigen. *Cancer Res* 1996;56:21–6.
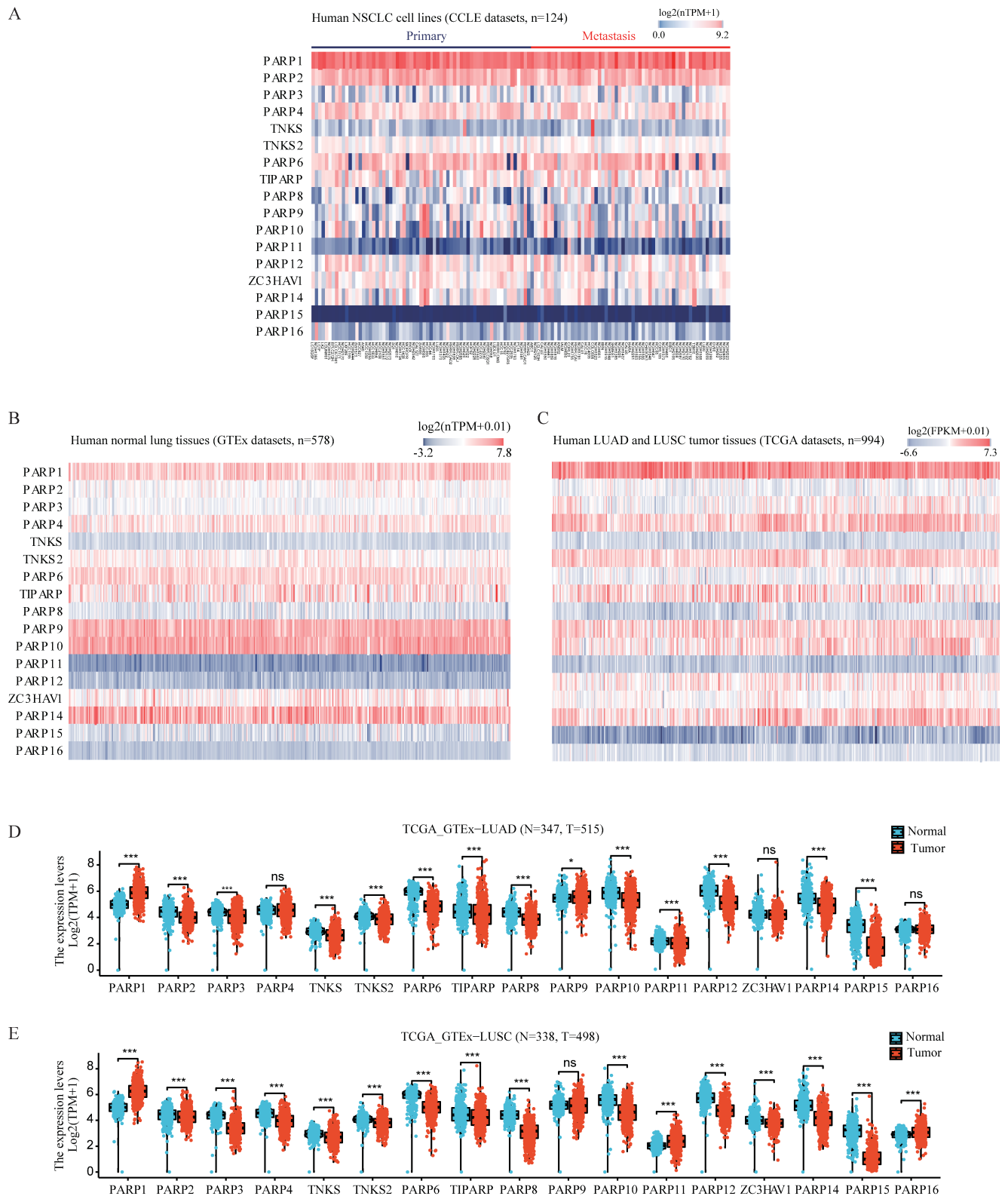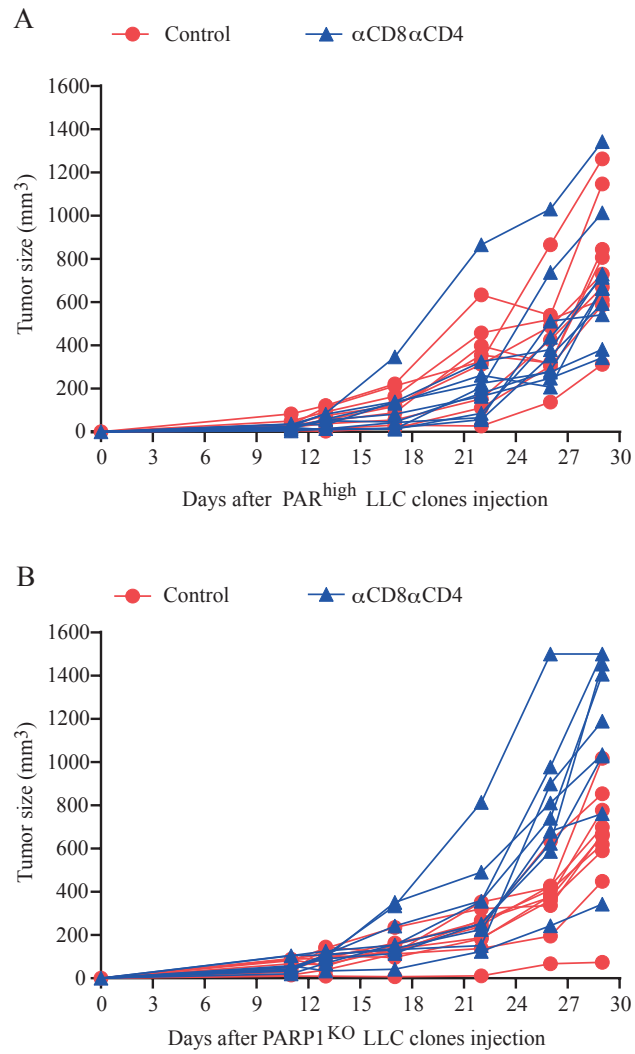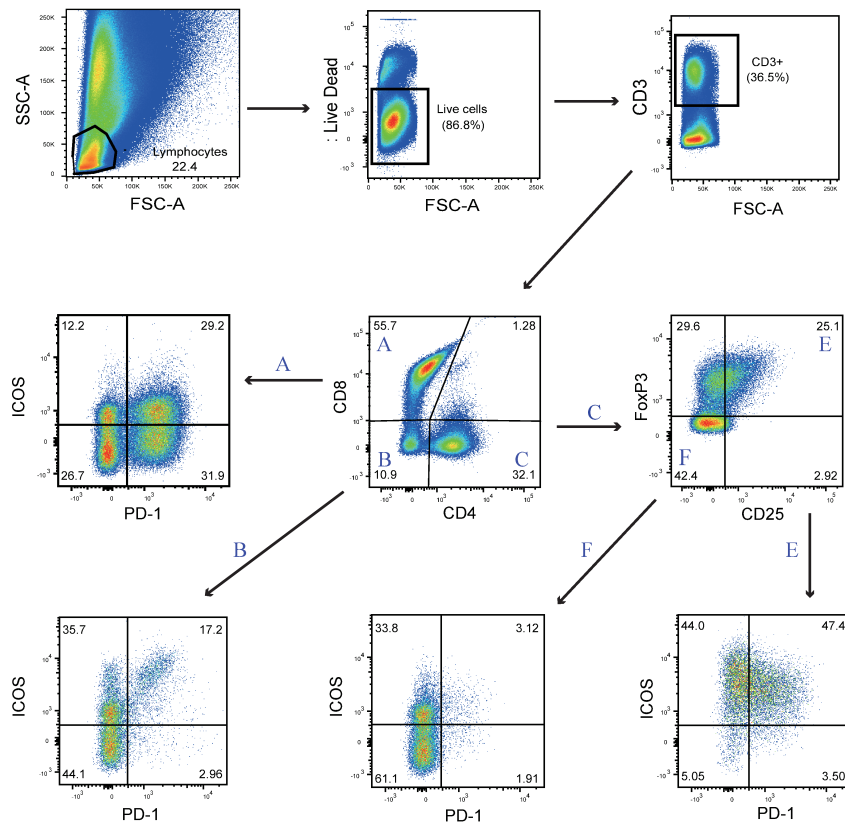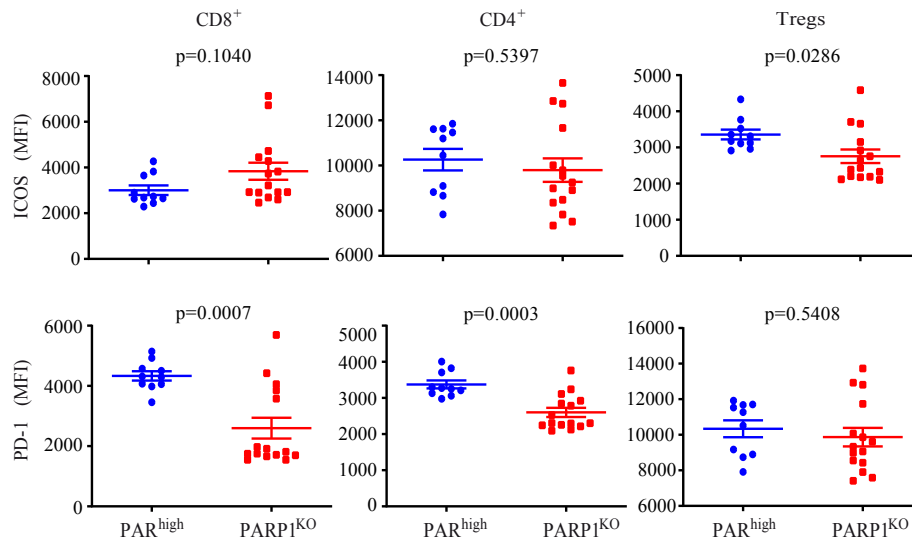
Supplemental figure 1

Supplemental material

BMJ Publishing Group Limited (BMJ) disclaims all liability and responsibility arising from any reliance placed on this supplemental material which has been supplied by the author(s)

J Immunother Cancer

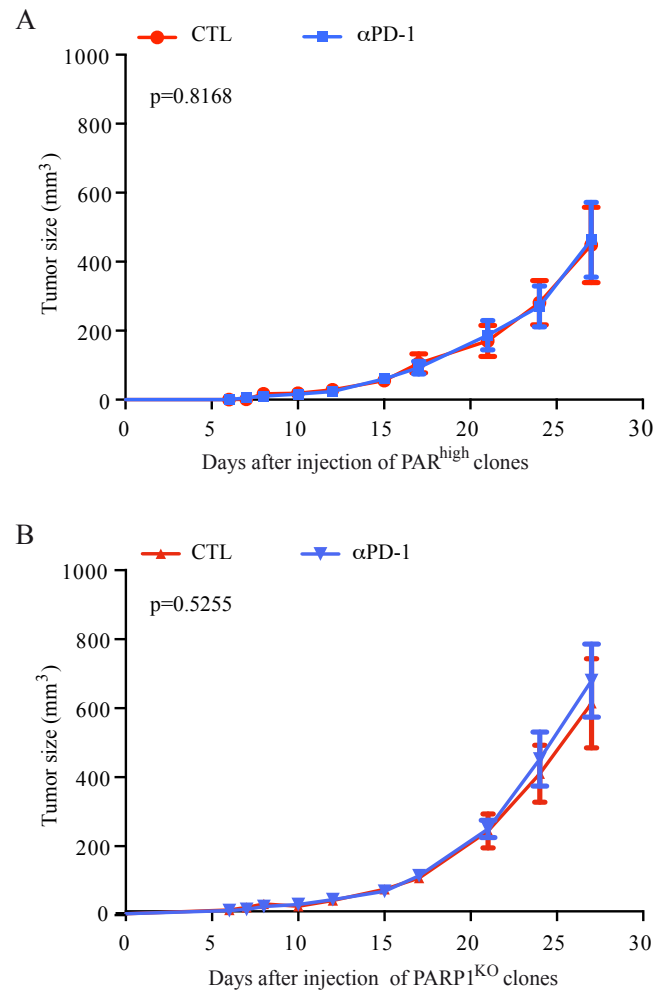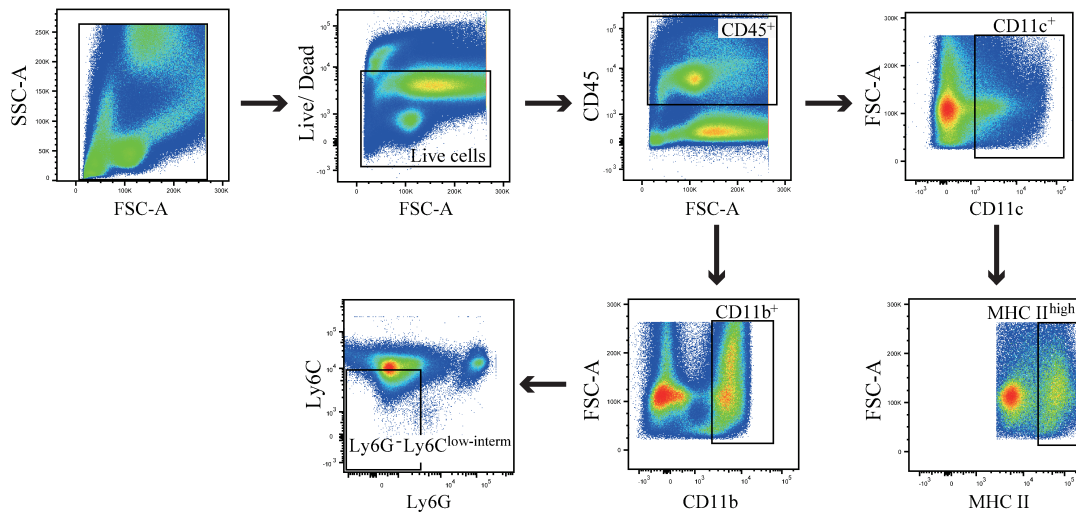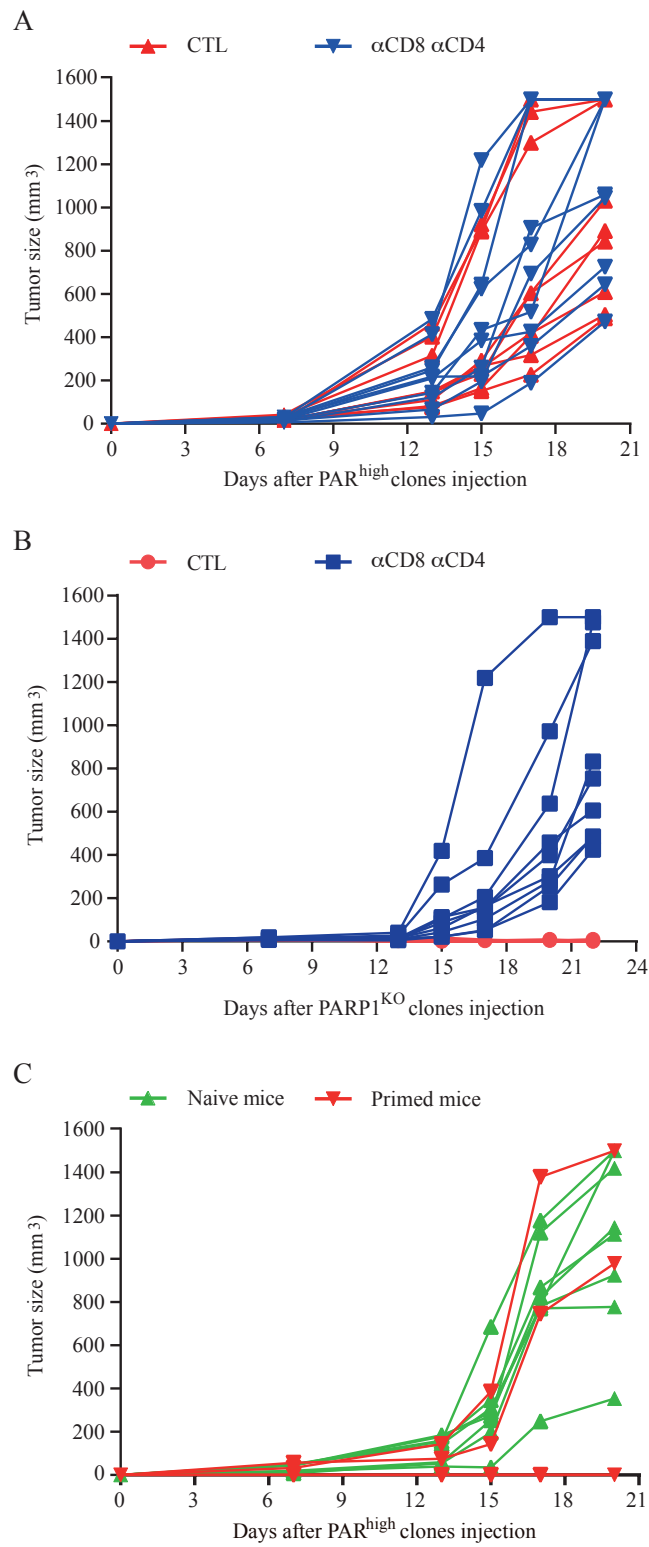**Supplemental figure 2**

Supplemental Figure 3

Supplemental figure 4

Supplemental figure 5

Supplemental material

BMJ Publishing Group Limited (BMJ) disclaims all liability and responsibility arising from any reliance
placed on this supplemental material which has been supplied by the author(s)

J Immunother Cancer

Supplemental Figure 6

A

B

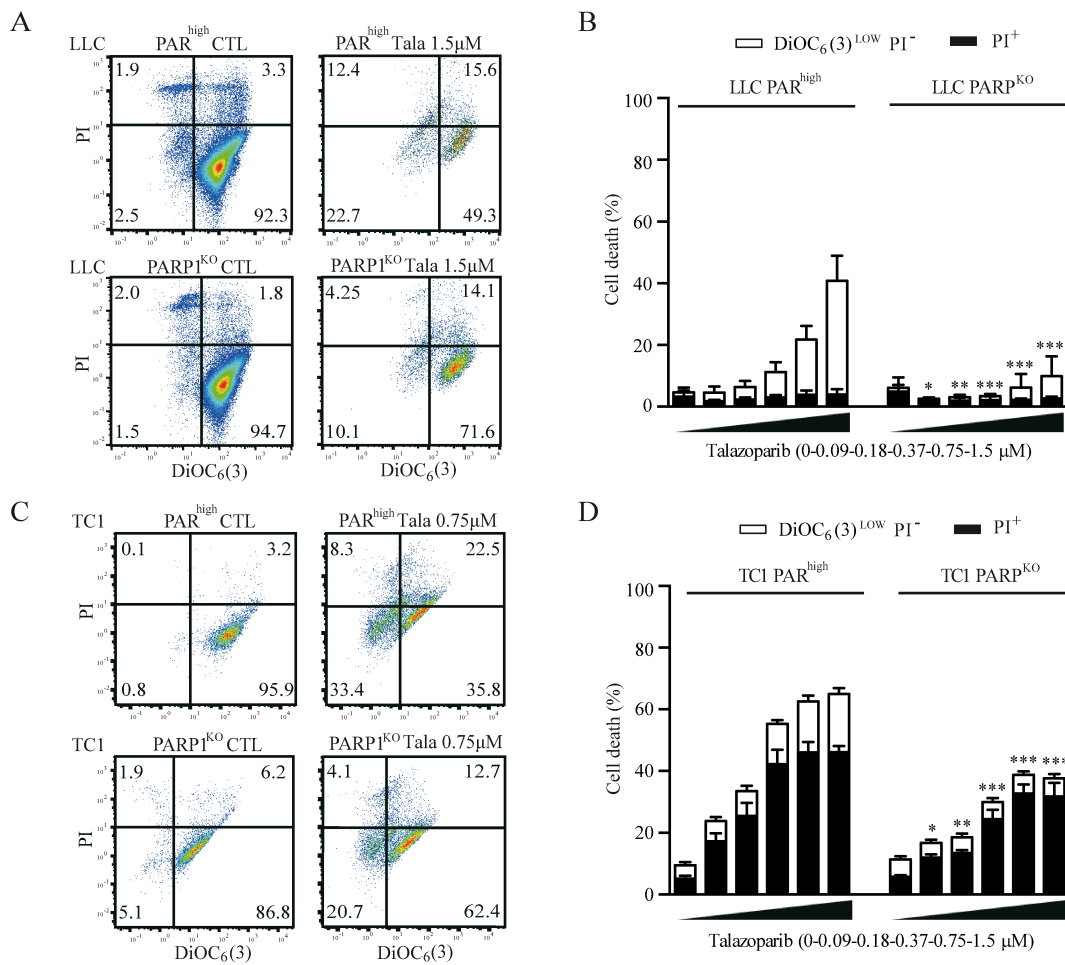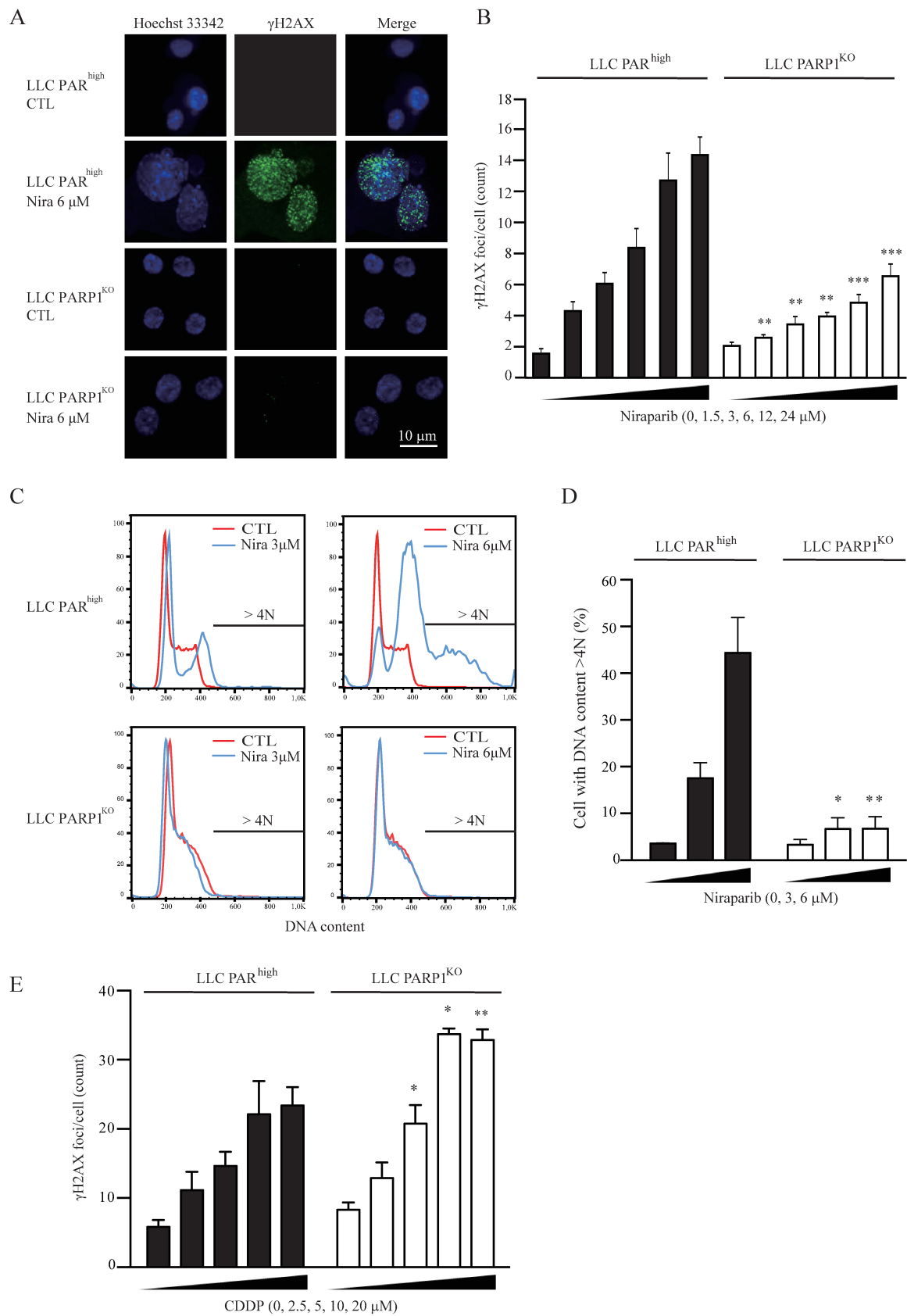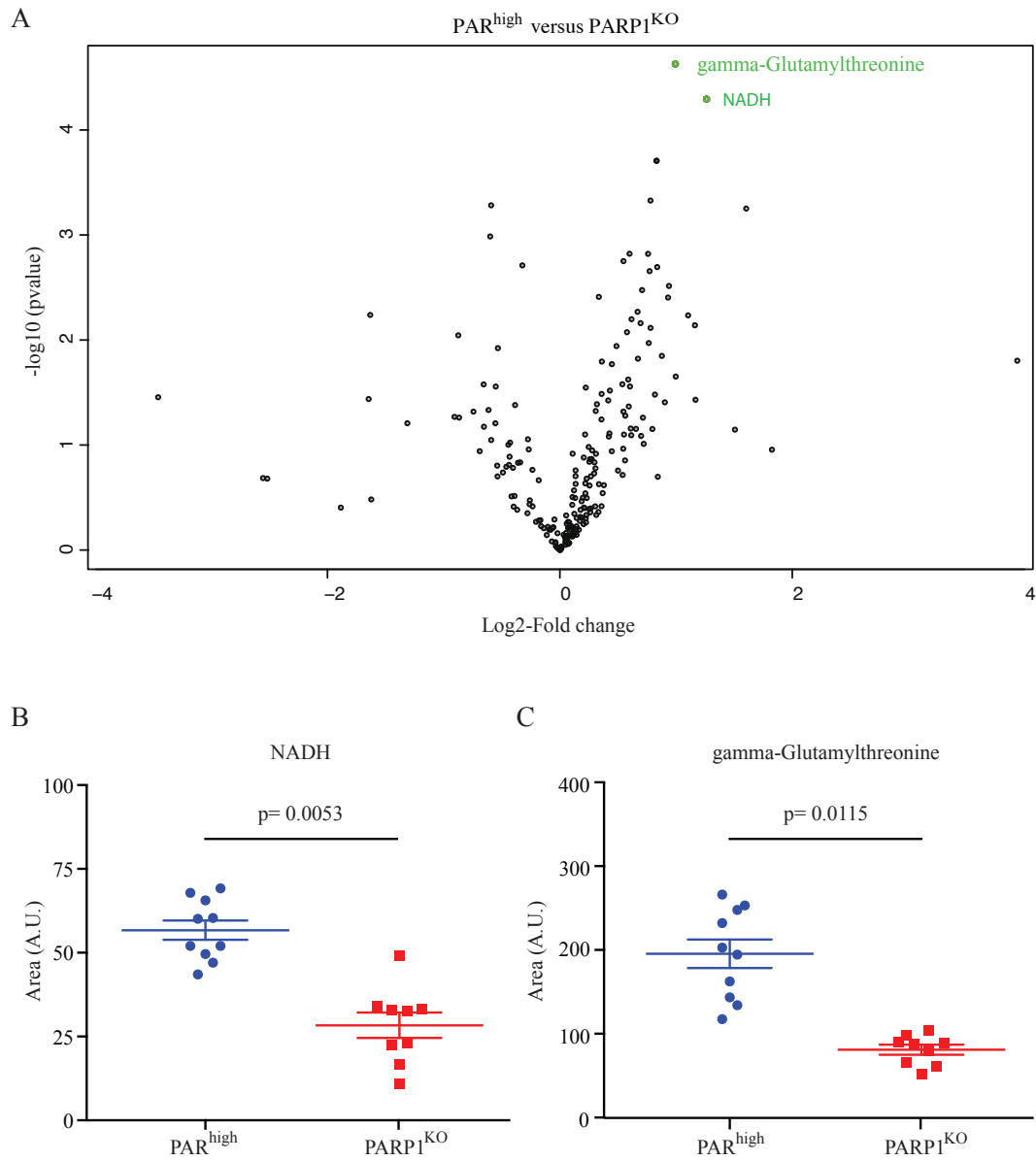**Supplemental figure 7**
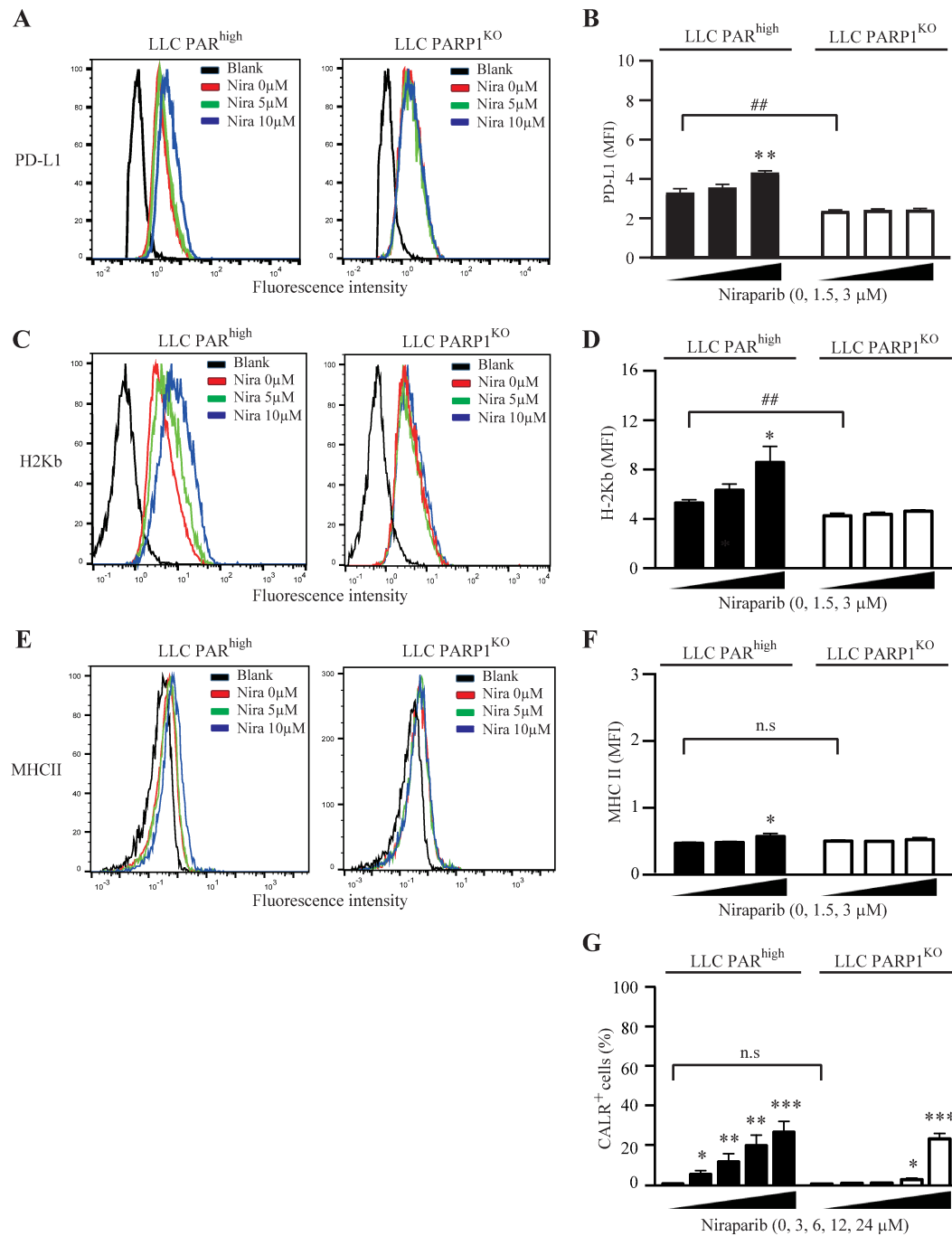
Supplemental figure 8

Supplemental Figure 9

Supplemental Figure 10
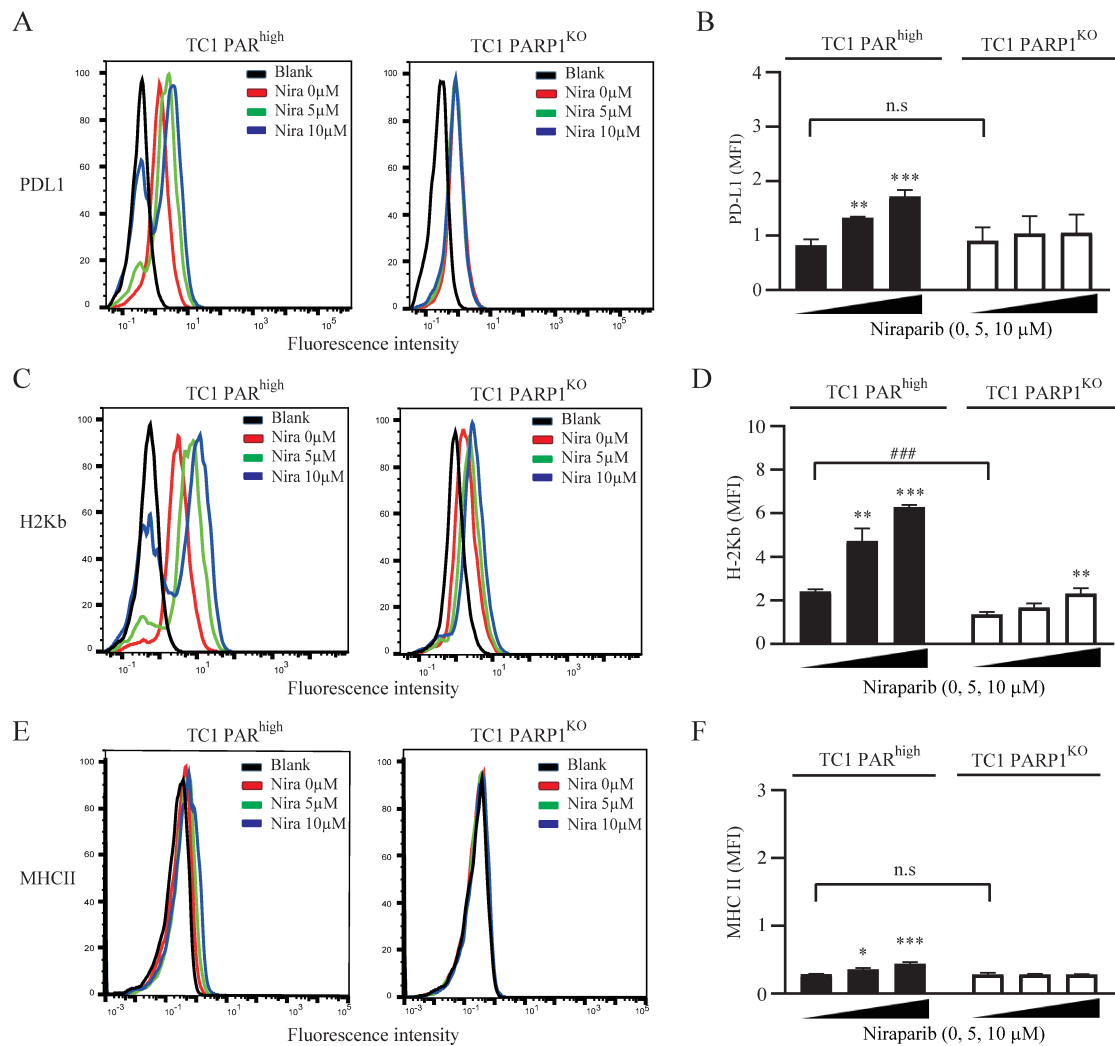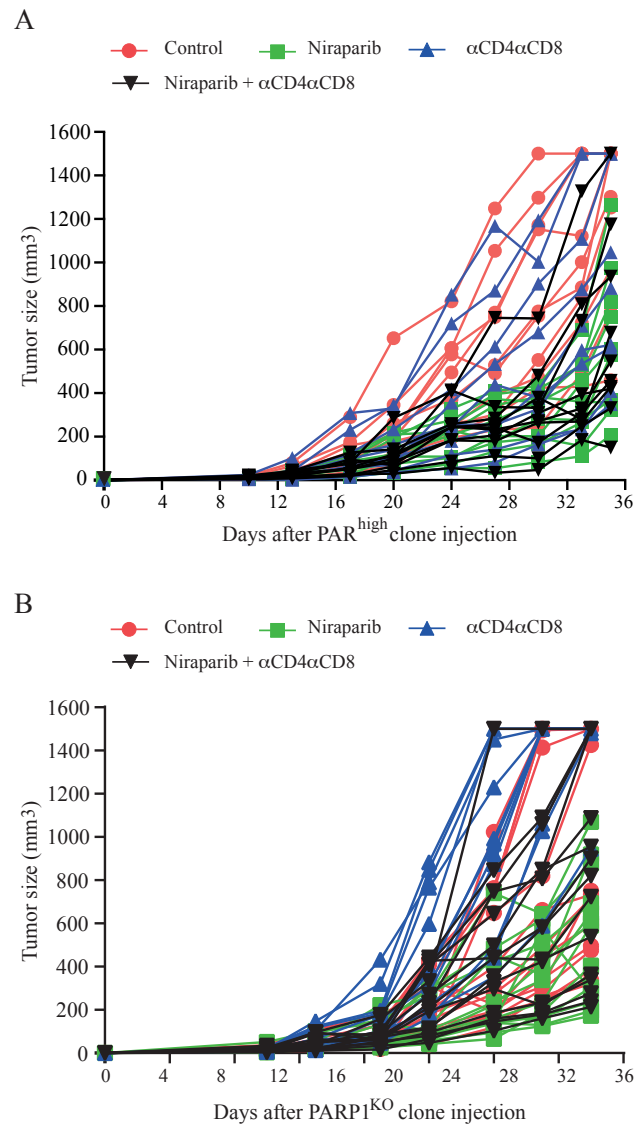
Supplemental Figure 11

Supplemental material

BMJ Publishing Group Limited (BMJ) disclaims all liability and responsibility arising from any reliance placed on this supplemental material which has been supplied by the author(s)

J Immunother Cancer

A

B

C

Supplemental figure 12

Supplemental material

BMJ Publishing Group Limited (BMJ) disclaims all liability and responsibility arising from any reliance placed on this supplemental material which has been supplied by the author(s)

J Immunother Cancer

Supplemental figure 13

Supplemental figure 14

Supplemental material

BMJ Publishing Group Limited (BMJ) disclaims all liability and responsibility arising from any reliance placed on this supplemental material which has been supplied by the author(s)

J Immunother Cancer

Supplemental figure 15

Supplemental figure 16

Supplemental material

BMJ Publishing Group Limited (BMJ) disclaims all liability and responsibility arising from any reliance placed on this supplemental material which has been supplied by the author(s)

J Immunother Cancer

Supplemental figure 17